ABSTRACT

Performance analysis of different packaging geometries of LFPC cells….. (to be added)

Table of Contents

Abbreviations

BOL	Beginning of life
DOD	Depth of discharge
ECU	Extended check-up
EFC	Equivalent full cycle
EOL	End of life
SCU	Short check-up
SOC	State of charge
SOH	State of health
SPICY	Silicon and polyanionic chemistries and architectures of Li-ion cell for high energy battery

1. Introduction

Lithium ion batteries have taken the most significant role in present day energy storage technologies and systems, primarily due to their high energy density and high specific energy. Invented by the American physicist Professor John Goodenough in 1980 as a new type of battery in which the lithium (Li) could migrate through the battery from one electrode to the other as a Li+ ion (Alarco and Talbot 2015), it was first commercially introduced as a product by Sony Corporation (Blomgren 2016). The simple basis of these batteries is that a compound of lithium with a transition metal - such as nickel, manganese, cobalt, iron - and oxygen forms the cathode, whereas, graphite is the anode (Alarco and Talbot 2015).
In terms of chemistry, Li-ion cells have an advantage over other technologies due to variety of reasons. Due to its lowest reduction potential of all elements, Li-ion cells have the highest available cell potential. Further, because of being one of the lightest element and having one of the smallest radii, Li-based batteries have high gravimetric and volumetric capacity and power density. (Nitta et al. 2015) Therefore, despite disadvantages like high costs and possible high temperature development, the above advantages make it very desirable for many commercial and research-related activities. This prompts for further studies and experiments to improve safety and reducing the costs of Li-ion batteries.

Saha and Goebel have summarized the lithium ion properties that makes it suitable for battery technologies as following:

- Li-ion batteries are made of lightweight lithium and carbon, making it lighter than other types of rechargeable batteries of the same type. Lithium itself is highly reactive and has potential to store high energies.
- Lithium ion batteries hold their charge for longer periods of time, that is they have low self-discharge.
- No memory effect, which means that Li-ion batteries do not have to be completely discharged before recharging to retain full charge capacity, which is the case in some battery chemistries like NiCd.
- Li-ion batteries have long cycle lives and can retain large number of charge-discharge cycles without significant losses in capacity.

However, lithium ion cells have a few disadvantages as well:

- The service life or shelf life of a Li-ion battery decreases with aging even if it is not used unlike other chemistries. This means that from the time of manufacturing, regardless of the number of times it was cycled, the capacity of a Li-ion battery will decline

gradually. This is due to an increase in internal resistance, which makes the problem more pronounced in high-current applications than low-current ones.

- They are more sensitive to high temperatures than most other chemistries. Hot storage and operating conditions causes Li-ion battery packs to degrade much faster than they normally would.
- Li-ion batteries can be severely damaged by deep discharge, i.e., by discharging them below the minimum voltage threshold recommended by the manufacturer (usually 2.7 V for a single cell). Consequently, Li-ion battery packs come with an on-board circuit to manage the battery. This makes them even more expensive than they already are.
- In general Li-ion chemistry is not as safe as NiCd or NiMH. This is because the anode produces heat during use, while the cathode produces oxygen (not for all Li-ion chemistries). Lithium being highly reactive can combine with this oxygen, leading to the possibility of the battery catching on fire.

The **Table 1** shows a comparison of Li-ion based batteries with others with different cathode materials.

Table 1. Comparison of Li-ion with other cathode materials in a battery

Cathode	**Li-ion**	**Pb-acid**	**Ni-Cd**	**Ni-MH**
Cycle life	500-1000	200-500	500	500
Working potential (V)	3.6	1.0	1.2	1.2
Specific energy (Wh/kg)	100	30	60	70
Specific energy (Wh/L)	240	100	155	190

Source: (Soylu 2011)

Currently, Li-ion technologies are used in a variety of applications, especially in portable electronics, hybrid/electric vehicles and power tools. The high energy efficiency of Li-ion batteries may also allow their use in various electric grid applications, including improving the quality of energy harvested from wind, solar, geo-thermal and other renewable sources, thus contributing to their more widespread use and building an energy-sustainable economy. (Nitta et al. 2015)

Because of Li's ability to form compounds with a variety of transition metals and oxygen, different types of Li battery technologies are available. **Table 2** shows some typical properties and their applications of the most commonly used types of Li-ion batteries:

Table 2. Typical properties and applications of some main types of Li-ion cells

	Li-Cobalt (LCO)	**Li-Manganese (LMO)**	**Li-Nickel Manganese Cobalt (LNMC)**	**Li-Iron Phosphate (LFP)**
Specific energy (Wh/kg)	150-200	100-150	150-220	90-120
Nominal voltage (V)	3.6	3.7	3.7	3.3
Cycle life	500-1000	300-700	1000-2000	1000-2000
Cost (USD/kWh)	-	-	420	580
Application	**Mobile phones, tablets, laptops, cameras**	**Power tools, medical devices, electric powertrains**	**E-bikes, medical devices, EVs, industrial**	**Portable and stationary needing high load currents and endurance**

Source: http://batteryuniversity.com/learn/article/types_of_lithium_ion

The advantages of lithium ion batteries far outweigh the disadvantages in terms of commercial application capabilities which necessitates the need for research to understand and alleviate the shortcomings of the technology and perfect.

2. Basics

Despite disadvantages like low electrical conductivity and slow Li-solid state diffusion and therefore, low specific energy and low capacity (Eftekhari 2017), LFPC is one of the safest Li-ion technologies and forms the basis of our studies in this work. It consists of $LiFePO_4$ as the cathode along with a graphitic carbon electrode in a metallic current collector grid as the anode. The following figure shows a schematic of the ion-transport inside an LFPC cell.

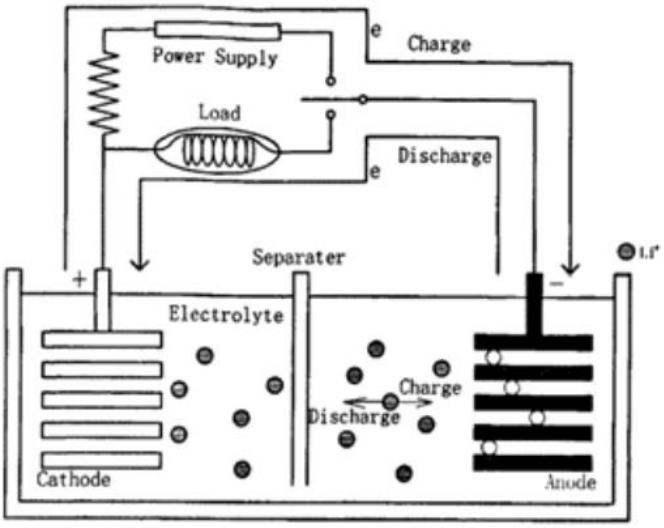

Figure 1. Schematic of the ion-electron transport in a Li-ion based cell (Soylu 2011)

The above figure shows the direction of electron flow in charging and discharging conditions. **……Equation 1** shows the extraction of Li-ion to charge the cathode, while **……Equation 2** shows the reverse process.

$$LiFePO_4 - x\ Li^{1+} - x\ e^- \rightarrow x\ FePO_4 + (1-x)\ LiFePO_4$$

……Equation 1 (Soylu 2011)

$$FePO_4 + x\ Li^{1+} + x\ e^- \rightarrow x\ LiFePO_4 + (1-x)\ FePO_4$$

……Equation 2 (Soylu 2011)

Apart from the electrode configuration, Li-ion cells can be divided into different types based on their geometry or the types of packaging of the electrodes with each other. The $LiFePO_4$-C are generally available in three main geometries: *cylindrical*, *prismatic* and *pouch* type.

Cylindrical geometry is the most common packaging technique for both primary and secondary cells. *"It has the main advantages of ease of manufacture and good mechanical stability. The tubular cylinder can withstand high internal pressures without deforming. Even though the*

cylindrical cell does not fully utilize the space by creating air cavities on side-by-side placement, the most common cylindrical cell dimension, the 18650, has a higher energy density than a prismatic/pouch Li-ion cell. The higher energy density of the cylindrical cell compensates for its less ideal stacking abilities and the empty space can always be used for cooling to improve thermal management. This cell design allows for added safety features that are not possible with other formats. It cycles well, offers a long calendar life and is low cost, but it has less than ideal packaging density. The cylindrical cell is commonly used for portable applications." (include reference of the webpage using Citavi Picker http://batteryuniversity.com/learn/article/types_of_battery_cells).

"Prismatic cells are encased in aluminum or steel for stability. Jelly-rolled or stacked, the cell is space-efficient but can be costlier to manufacture than the cylindrical cell. The prismatic cell improves space utilization and allows flexible design but it can be more expensive to manufacture, less efficient in thermal management and have a shorter cycle life than the cylindrical design." (same reference as cylindrical cells above)

"The pouch cell offers a simple, flexible and lightweight solution to battery design. Some stack pressure is recommended but allowance for swelling must be made. The pouch cells can deliver high load currents but it performs best under light loading conditions and with moderate charging. It is cost-effective but exposure to humidity and high temperature can shorten life. Adding a light stack pressure prolongs longevity by preventing delamination. Swelling of 8–10 percent over 500 cycles must be considered with some cell designs." (same reference as cylindrical cells above)

Figure 2 below shows diagrammatically the different geometries of Li-ion cells

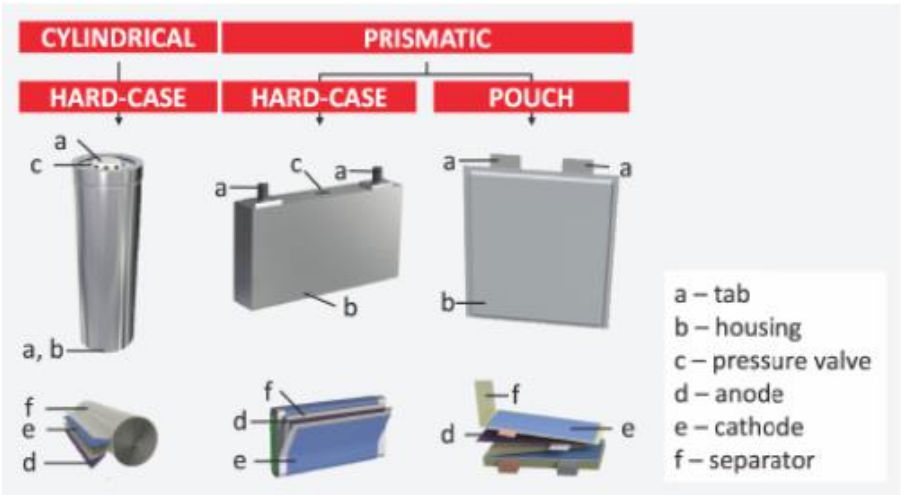

Figure 2. Diagrammatic representation of types of Li-ion packaging geometries (Schröder et al. 2017)

The **Table 3** below shows a comparison between the cell geometries with respect to their advantages, disadvantages and their applications.

Table 3. Comparison of cell packaging geometries

	Cylindrical	Prismatic	Pouch
Advantages	Ease of manufacture Good mechanical stability Withstand high internal pressure without deforming Lower cost (watt per hour) Long calendar life and cycling ability Higher energy density	Thin profile (effective use of space) Light weight Allows flexible design Encased in metal or steel for stability	Similar to prismatic cell except no need for metallic casing Most efficient use of space Light weight
Disadvantages	Notable space between cells (less space efficiency) Heavy Low packaging density due to space cavities	More expensive to manufacture Difficult and less efficient in thermal management Shorter cycle life Deformation in high pressure situations	Provision for swelling must be made Similar to prismatic cells

		Higher cost (watt per hour)	
Applications	Power tools, medical instruments, laptops and E-bike	Mobiles phones, tablets and low-profile laptops Electric powertrains in hybrid and electric vehicles, electric buses, trucks, solar/wind storage UPS	Portable applications like drones and hobby gadgets Energy storage systems (ESS)

Source: https://www.slideshare.net/AnmolJaggi/comparison-between-different-li-ion-cells-type

In this work, a study has been done on the experiments done on various generations of LFPC cells. The different generations indicate different modifications done on either of the electrodes to improve the capacity and energy density of LFPC and then, analyzing the experiments results to determine the performance changes for the different packaging geometries of the cells.

(Saha and Goebel 2009) Definitions:

- C-rate: Expressed as C/r, it is the rate at which a cell can be charged or discharged in r hours. Units: Ah. For example, to charge a 2Ah in 1 hour would require 1C or 2A of current, while to discharge a 2Ah battery in 4 hours, C/4 or 0.5A of current should be drawn.
- Specific energy: This refers to the energy per unit weight. Unit: Wh/kg
- Specific power: This refers to the power per unit weight. Unit: W/kg
- Energy density: This refers to the energy per unit volume of the cell. Unit: Wh/m^3
- Power density: This refers to the power per unit volume of the cell. Unit: W/m^3
- Cycle life: The number of times a cell can be discharged and charged again, that is undergo a full cycle, until the capacity has faded to end of life limits, typically 80% of original capacity in automobile applications.

- Coulombic efficiency: Denoted by η_c, it is defined as the fraction of the prior charge capacity that is available in the following discharge cycle. It depends on current, depth of discharge and the temperature.
- Self-discharge: The process of discharge of a stationary battery not subjected to any loads and is caused by the residual ionic and electronic flow through a cell even when there is no external current being drawn

3. State of the art

Lithium-ion cells are taking over the storage market from low power to high power applications. As discussed already, due to the chemical properties of lithium, these cells can be produced with many different selections of cathodes and anodes and in various sizes. There is further evidence in benefits of using $LiFePO_4$ based cathodes and its increasing importance. Many studies have been done to compare the different chemistries of Li-ion cells and even different sizes in terms of geometries.

On the other hand, studies on the packaging geometries of the Li-ion cells are limited. Pouch based packaging geometries, for e.g., are finding lot of applications in EVs and HEVs and are even replacing cylindrical cells in many cases because the improved energy density and low weight due to its lightweight outer covering. A limited number of studies include a thorough comparison based on its performance analysis with respect to parameters like capacity evolution, internal resistance developed, differences in chemical changes during cycling, among others. This chapter discusses the state of the art in research for the comparison study between the cell packaging geometries. The literature reviewed in this study is not just limited to LFPC and Li-ion cells, but tries to incorporate relatable results from the work on other electrochemical cells as well.

(Ahn et al.)A physical and geometrical comparison of the three packaging types can be found in the work done by Ahn et al. It compares the physical constraints of jelly roll wound types (cylindrical and prismatic) with flat stacked designs (pouch) for Lithium-polymer cells. In the case of jelly roll configurations, the metal enclosure of slimmer batteries (for e.g. prismatic cells) do not exert enough pressure onto the electrodes and results in poor thickness control. It also enumerates some of the advantages of a flat design: maintaining uniform battery thickness, higher energy densities due lower dead volume and lower cell impedance due to the plurality of electrical contacts through electrode tabs. Further, free stack structures without any folding options, which specifies the pouch type cells, allow the separator materials to contract when exposed to shutdown temperatures, which results in triggering safety events more easily around the electrode edges. The work illustrates the need for studying of cell designs for safer lithium ion battery technology.

The work by Maiser 2014 gives a (Maiser 2014) brief overview of battery packaging concepts, their specific advantages and drawbacks, as well as the importance of packaging for performance and cost. It concludes that while the front-end production have the highest impact on the cost of the battery, back-end design and processing (packaging) adds important safety and intelligent control features without which Li-ion batteries would not be

manageable. It also reviews a brief history, characteristics and applications of the three packaging geometries relevant to this work: cylindrical, prismatic and pouch.

Mulder et al. have done a comprehensive study on the comparison of commercial Li-ion battery technologies with different chemistries and packaging geometries. The work evaluates the behavior of these cells for automotive applications like plug-in hybrid vehicles and battery electric vehicles, where tests for high power and high energy applications are included. Within the scope of this study, commercial cells of different geometries were also studied and a comparison was made (Mulder et al. 2013). It was concluded that pouch cells behave better than average with respect to the power efficiency, whereas due to design factors, the prismatic shape has a clear negative effect on the efficiency. Prismatic cells also seem to have a clear negative effect on efficiency, as it becomes the hottest, while cylindrical cells warm up less. Further, pouch cells show the highest power densities. While this work is comprehensive and includes many parameters for comparison, it does not necessarily include whether the cells from the three packaging geometries have the same internal chemical composition and design capacities.

Further literature studied for this work involved studies on capacity evolution, aging parameters, internal resistances, temperature developed and pulse polarization tests of Lithium-ion cells. The following part discuss in detail the various aspects related to capacity deterioration and overpotentials along with the associated resistances.

The cyclic ageing and capacity deterioration of Li-ion cells depends on a variety of factors as enumerated by Zhao: loss of lithium ion-inventory, loss of active material, ohmic resistance increase, lithium plating among others. These mechanisms are discussed further in detail by Anseán González. Barré et al have reviewed the ageing mechanism, and ageing battery estimation methods in Li-ion batteries. Sarasketa-Zabala et al provide a detailed analysis of the influence of DOD, C-rate and Ah-throughput on cell ageing of LFPG cells. Pinson and Bazant discuss the theory of solid electrolyte interface (SEI) in rechargeable batteries: capacity fade, accelerated aging and lifetime prediction.

Many literatures study the ageing characteristics of Li-ions cells and discuss the involved mechanisms, although the mechanisms may differ from one chemistry and cell geometry to other. The work done by Sikha et al. discusses the capacity fade of cylindrical 18650 Li-ion cells at different charge-discharge protocol. For the constant current – constant voltage (CC+CV) and constant voltage (CV) protocol, that has been used in this thesis work, the short time during which the current is very high while charging using CV protocol is responsible for increased capacity fade (Sikha et al. 2003). Many of the known work is done for the case of commercial cylindrical cells. Han et al. investigated different commercial Li-

ion cells and concluded that the ageing mechanism differ with different chemistries of the cells. (Han et al. 2014) Two LFPC cells were investigated in this study and it was observed that the battery aging mainly arises from the loss of lithium inventory and loss of the anode active material, while in another case despite lithium inventory loss, no significant anode or cathode loss was observed. Sun et al. studied the degradation mechanism with respect to the cycle lifetime of commercial $LiFePO_4$/Graphite cells at different ambient temperatures and observed that the mechanism changes for different temperatures. (Sun et al. 2017)While at room temperatures, the capacity fade is due to active lithium loss by generation and reformation of solid electrolyte interface (SEI) film, at temperatures above 35°C, the electrolyte decomposes which results in accelerated consumption of active lithium. Elevated temperatures have an adverse influence on the performance of $LiFePO_4$ material. Further many literature works have explored the use of differential voltage analysis (DVA) to studying aging. One among them, Lewerenz et al., uses DVA for calendar and cycling ageing of cylindrical LFPC cells and focusses on mechanisms of homogeneity of active lithium distribution and loss of active anode material. (Lewerenz et al. 2017)They arrive at the conclusion that for cyclin ageing, several phenomena are correlated to degradation, such as loss active lithium, local loss of active anode material for depth of discharge (DOD) 100%, deactivation of certain layers of anode and cathode due to a lithium-permeable covering layer on top of the anode. The literature review of the ageing in different cells revealed many different trends for different cells. Despite that not much work has been done for the distinction of ageing among Li-ion cells based on packaging geometries with cylindrical cells being the most popular geometry for research.

Has summarized the different ageing mechanisms in Lithium-ion batteries as follows:

- Loss of lithium inventory (LLI): LLI leads to loss of Li ions due to parasitic reactions, though it does not change the content of active materials in electrodes and their properties. It is reported to be the major cause of degradation of lithium-ion batteries. It is attributed to two main causes: the primary cause is the SEI layer formation, growth and destabilization, and the secondary cause of side reactions of lithium ion with decomposed electrolyte compounds and water in the electrolyte. LLI occurs chiefly at the electrode/electrolyte interface and is predominant on the negative electrode where SEI formation dominates. SEI growth and subsequent LLI is dependent on temperature: at high temperatures, the SEI either grows in thickness or becomes non-protective leading to performance degradation, whereas at low temperatures, the risk of lithium plating leads to cell degradation.

- Loss of active material (LAM): It directly affects the structure of the electrodes, reducing the volume of active material used in the cell and the ageing effects in this case are more prominent in graphite based negative electrodes than positive electrodes. It is enhanced by high currents, high temperatures and high SOC. The major reasons of LAM are: particle isolation, side reactions within the active material of the electrodes and physical degradation. LAM may lead to second stages of cell degradation where abrupt capacity losses might appear after steady capacity loss in the first stage.
- Ohmic resistance increase (ORI): Degradation caused on the electrodes and electrolyte materials directly result in the increase in the electronic and ionic resistances, respectively. The possible reasons for ORI are particle isolation causing LAM, binder decomposition, current collector corrosion, volume changes in active material and electrolyte contamination, SEI growth, destabilization affecting ionic resistance.
- Lithium plating: This occurs during charging when lithium ions deposite on the negative electrode instead of intercalating into the graphite. It is the most detrimental aging mechanism as it also leads to safety deterioration. It can result from large number of factors, like constructive properties of the cell to operating conditions (like low operating temperatures and high current rates). Li plating increase LAM and LLI.

Further, to understand the pulse test (explained in next chapter) results, the polarization and overpotential concepts were studied. Polarization discharge curves are a popular way to study the behavior of a cell during discharge of a non-rechargeable battery, especially fuel cells. DuBeshter and Jorne have discussed a way to develop pulse polarization curves (PPC) for a Li-Ion battery under constant SOC to identify individual over-voltages, such as charge transfer kinetics and mass transport, and their SOC dependence. In this work, different time scales of a discharge pulse have been formulated to represent the kinetic overpotential, electrolyte Li+ concentration and Li solid state diffusion.

Saha and Goebel have done a study on the modeling of Li-ion battery capacity depletion in a particle filtering framework and have further described the battery characteristics and the concept of overpotential in their work. Park et al. have done a review of the conduction phenomena in Li-ion batteries. (Saha and Goebel 2009) The cell potential is calculated as the difference of the Gibbs free energies the product of the reactants and products (potential difference between the electrodes), with the theoretical open circuit voltage, E^o, measured with the reactants at 25°C and 1M solutions. This is the equilibrium potential. But

during the operation of the battery, due to current flow or charge flow, the potential deviates from the equilibrium and this shift is known as the polarization. In the case of oxidation (loss of electrons), the actual potential is more than the equilibrium potential, while the vice-versa is true for reduction (gain of electrons). (Saha and Goebel 2009) This shift or voltage drop is due to various passive components inside the electrolyte, the separator, the terminal leads etc., which are characterized as the following factors:

i. Internal resistance (IR) drop: Voltage drop associated with the internal resistance of the battery during the current flow across the terminals. The internal resistance has been categorically divided in **Table 4**.
ii. Activation polarization: This involves the kinetics involved with the electrochemical reaction, like the work function that the ions must overcome at the junction between the electrodes and electrolytes. It is associated with the kinetics of charge transfer.
iii. Concentration polarization: The potential drop associated with the mass transfer resistance (e.g. diffusion) during the ion transportation across the electrolyte from one electrode to another. It is associated with the kinetics of mass transfer.

This can be mathematically denoted using the following equation:

$$(Park\ et\ al. 2010)\ E = E_0 - [(\Phi_{ct})_a + (\Phi_{ct})_c] - [(\Phi_c)_a + (\Phi_c)_c] - iR_i = iR$$

where, E_0 is the standard cell potential, $(\Phi_{ct})_a$, $(\Phi_{ct})_c$ are activation polarizations (charge-transfer over voltage) at the anode and cathode, $(\Phi_c)_a, (\Phi_c)_c$ are concentration polarizations at the anode and cathode, i is the cell operating current, R_i is the internal resistance of the cell and R is the apparent cell resistance.

Liu et al. have studied the differences in electrochemical potentials in different rechargeable batteries and have summarized the differences in the case if lithium based electrodes as compared to other technologies. (Liu et al. 2016)In typical galvanic batteries, the redox reactions proceed simultaneously with the receding or advancing of the electrode surfaces, but not accompanied by either the solid-state mass diffusion in the electrodes or a change in the chemical composition and local atomic environment. By contrast, the heterogeneous redox reactions in Li-ion batteries are always accompanied by solid-state mass diffusion as well as volume expansion or contraction, although the electrode surfaces do not recede or advance when the volume change of electrodes is not considered. Therefore, it is very reasonable that researchers face different challenges when developing Li-ion batteries, necessitating different fundamental considerations. Li ions, the working ionic component of electrochemical reactions, are transferred back and forth between the anode and the cathode through the electrolyte. While the concentration of lithium ions remains

constant in the electrolyte regardless of the degree of charge or discharge, it varies in the cathode and anode with the charge and discharge states.

Figure 3 below shows a schematic of a rechargeable Li-ion cell to demonstrate the movement of ions within the cells. (Liu et al. 2016) For a Li-ion battery, as illustrated in the figure, Li ions are extracted from the cathode and inserted into the anode during the charge process, and the reverse reaction occurs during the discharge process. However, in a half-cell consisting of electrode material and lithium metal, Li ions are extracted from the electrode material and deposited on the surface of the lithium metal during the charge process, and Li ions are inserted into the host electrode material during discharge. Here, in practice, the electrode materials can be cathodes or anodes.

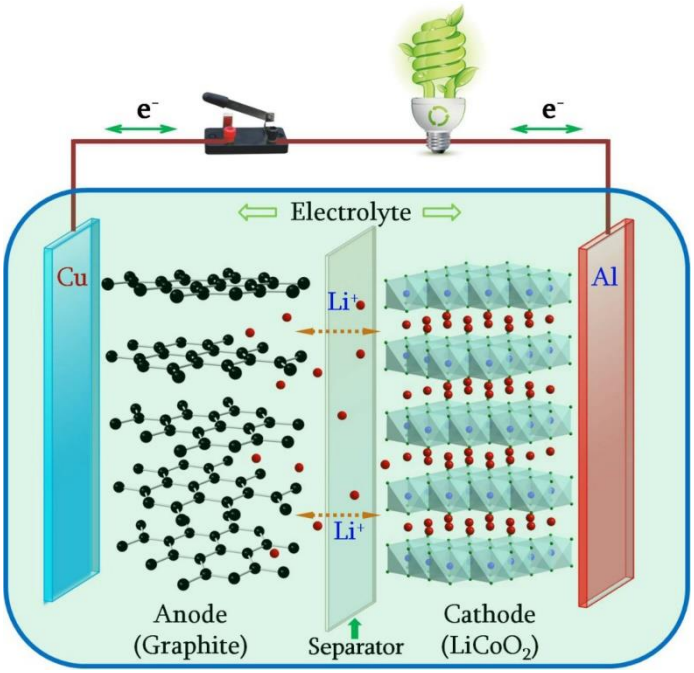

Figure 3. An example schematic of a rechargeable Li-ion battery to explain the transfer of ions within the cell (Liu et al. 2016).

Liu et al. further summarize that an SEI film permits the diffusion of Li ions through the film under a uniform electric field and reduces the overpotential and concentration polarization. The SEI can also prevent the aggregation of electrochemically active particles and maintain a uniform chemical composition at the electrodes. For example, the SEI can effectively prevent the exfoliation of graphite during the insertion and extraction of lithium ions. However, the SEI film increases the internal resistance of the battery and consumes part of the Li ions from the cathode, leading to both power and capacity loss. This helps in correlating the SEI film formation with both the polarization process, internal resistance increase and capacity losses.

The internal resistance of a cell can be categorized as shown in **Table 4** below:

Table 4. Types of internal resistances

Type of resistance	**Internal resistance of cell, R_i=ionic resistance + electrical resistance + interfacial resistance**
Ionic	• Electrode particle • Electrolyte
Electrical	• Electrode particle • Conductive additives • Percolation network of additives in electrode • Current collectors • Electrical taps
Interfacial	• Between electrolyte and electrodes • Between electrode particles and conductive additives • Between electrode and current collectors • Between conductive additives and current collectors

(Source: (Park et al. 2010))

Park et al. have done a review of the electrical and ionic conductivity separately for anodes and cathodes, especially with interesting insights into $LiFePO_4$ based cells. Doping does not affect the electrical conductivity of $LiFePO_4$. Electrical conductivity is found to have a larger value than ionic conductivity in LFPC cells, therefore ionic conductance dictates electrochemical performance, which explains why electrical conductance of $LiFePO_4$ is not affected by doping or solid-state reaction conditions. The study further discusses the chemical processes involved during conduction in a cathode. **Figure 4** depicts such a case for $LiFePO_4$ based cathode. When a Li-ion diffuses out of the cathode (ionic conduction) during the charge cycle the valence state of the transition metal ion changes (electronic conduction), the Fe^{2+} ion is oxidized to Fe^{3+}. Assuming diffusion governs charge/discharge rates, ionic conductivity is

more significant than electronic conductivity because high ionic conductivity will allow rapid diffusion of Li-ions into the cathode materials in the case of charging.

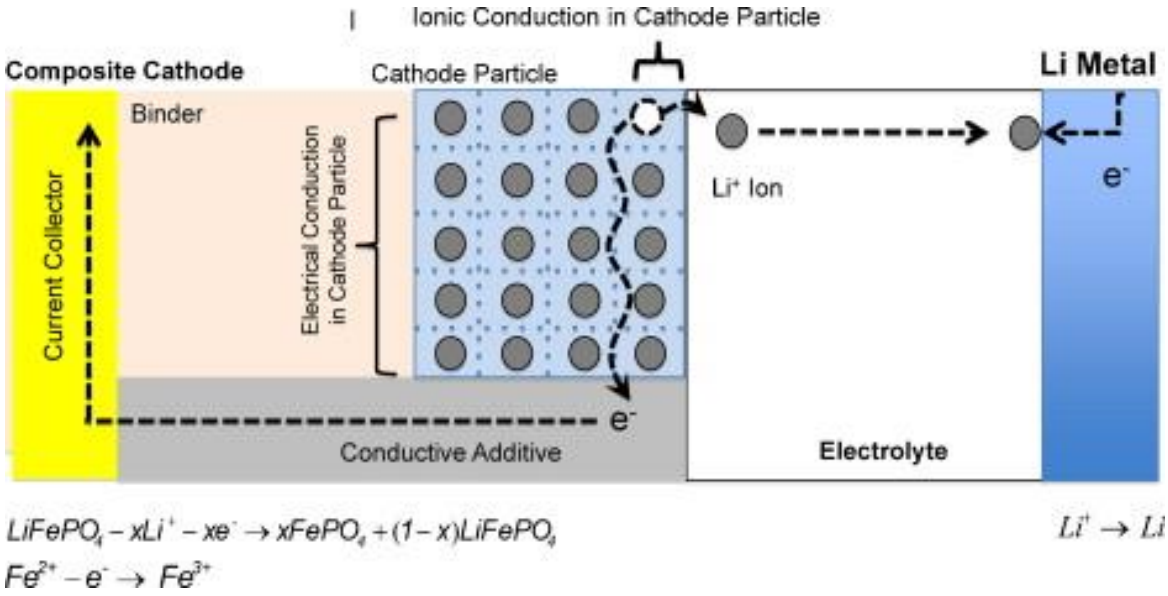

Figure 4. Conduction phenomena in a single composite cathode particle of a $LiFePO_4$ cathode during charging (Park et al. 2010)

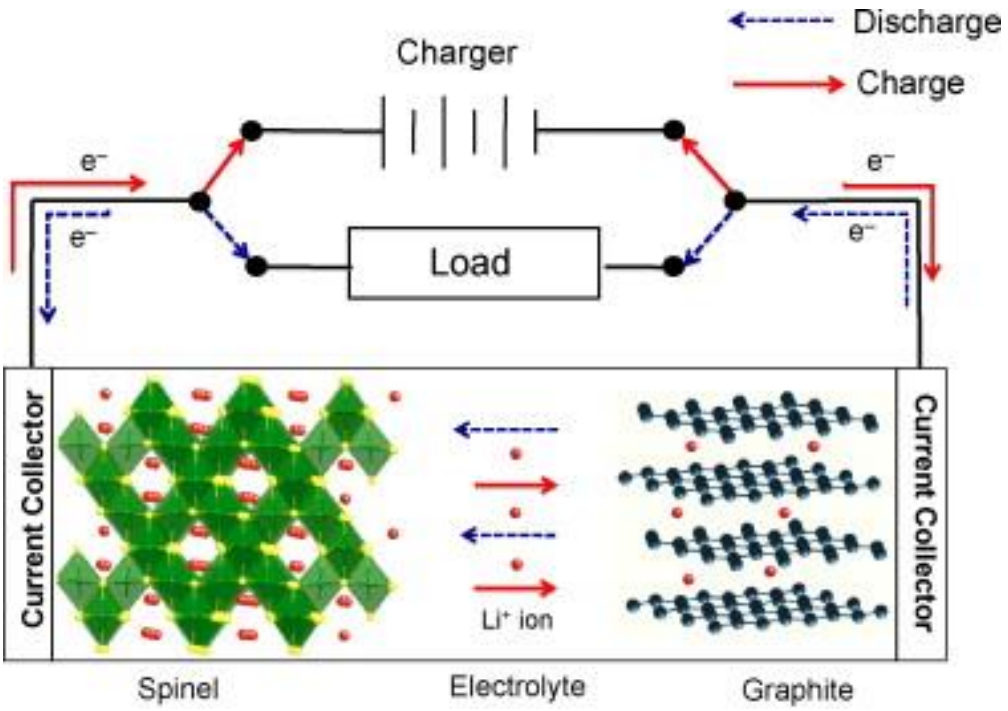

Figure 5. Schematic diagram to show intercalation and de-intercalation of Li ions in the presence of a graphite based anode (Park et al. 2010)

(Park et al. 2010) Conduction in graphite anodes is complex due to the continuous phase transformations and the formation of SEI layers. A prominent feature of graphite anodes is the staged intercalation of Li-ion, and the diffusivity of Li-ions in graphite is found to be a function of intercalation or electrical voltage. **Figure 5** shows a schematic to represent the intercalation of Li-ions in the graphite during charging. It is concluded that major features of conduction in the anode are closely related to phase transformations as a function of Li-ion intercalation and SEI layer formation.

4. Experimental Setup

The collaborative research project, SPICY (acronym for Silicon and polyanionic chemistries and architectures of Li-ion cell for high energy battery) aims at development of new generation of Li-ion batteries with respect to performance, safety, costs, recyclability and lifetime. It particularly involves performance improvement of $LiFePO_4$ based on LFPC cells. "$LiFePO_4$ is well known as a safer and more durable cathode material. Unfortunately, its energy density is low due to the electrochemical potential of Fe. One objective of SPICY will be to bind metals having a higher potential than Fe, allowing an increase of the material potential, and thus a higher energy." (SPICY Innovative Battery 2015)

"One of the main objectives in SPICY is to work on the family of polyanionic phosphates bound to metals. This active material allows higher potentials resulting in an increased energy density and reduced battery weight." (TUM-Institute for Electrical Energy Storage Technology, SPICY Homepage 2018)

For the thorough comparison of Li-ion cells, cells of different geometries have been manufactured. This gives the opportunity to compare the performance capabilities of the three geometries for same materials and conditions of the cells. Literature on comparison of cell packaging geometries for cells of same chemical composition and size is limited and therefore, it has an elevated scope for research.

In this chapter, the experimental setup is discussed. In the first part, the cell geometry, size and chemical composition of the cathodes and anodes are mentioned. The second part describes the test performed on the cells which are used in scope of this thesis work.

4.1. Cell chemistry

To have a common comparison standard between the cell packaging geometries, the chemistry for the anode, cathode, electrolyte and separator were chosen to be the same. All cells have been manufactured have the same material for the electrodes, i.e., $LiFePO_4$ as the cathode and graphite as the anode. Both the materials of the electrodes are from the same batch of raw materials for all the cells (Include SPICY Deliverable 5.6).

The separator, as already discussed, isolates the two electrodes and is a membrane that allows transfer of ions from cathode to anode on charge (reverse on discharge). The small current passing through the separator constitutes the self-discharge and gradually reduces the cell capacity. The separator used for the cell manufacture is a tri-layers Celgard 2325 grade. This type of tri-layered poly-olefin separator consists of 1 polyethylene (PE) layer sandwiched

between two layers of polypropylene (PP), and is the most commonly used separator type. This is because of their chemical inertia and the safety feature the combination of PP-PE-PP offers. In the case of overheating, the PE layer melts, losing its porosity (i.e., mechanically blocking the Li+ ion movement), while the PP layer prevents large dimensional changes until its own melting, thus preventing short-circuits. The Cellgard 2325 has a thickness of 27 µm and an air permeability defined by a Gurley number of 570s. (Kirchhöfer et al. 2014) Gurley number is defined as the number of seconds required for 100 cubic centimeters (1 deciliter) of air to pass through 1.0 square inch of a given material at a pressure differential of 4.88 inches of water (0.176 psi) (ISO 5636-5:2003). (Hutten 2007)

The composition of the electrolyte solution strongly influences the temperature dependence of the capacity. This is related to the quality of the passivation of the graphite electrodes in the various solutions and to the transport properties of the passivating surface films that cover the graphite particles (Yaakov et al. 2010). For the cells manufactured by SPICY, the electrolyte solution used is a blend of ethylene carbonate (EC), propylene carbonate (PC) and di-methyl carbonate (DMC) in volume proportion 1:1:3, respectively, with 1M of LiPF6 and 2% weight of vinylene carbonate (VC). (Include SPICY Deliverable 5.6)

4.2. Cell geometry and size

The three packaging geometries (cylindrical, prismatic and pouch) were assembled in different ways, which are mentioned in the SPICY Deliverable 5.6.

Jelly roll manufacturing was used to wind together the electrodes and separator in cylindrical and flat cores ***for cylindrical and prismatic cells***, respectively. While the cylindrical cores are basically rolls of electrodes with separators within them, for the prismatic cells, the cores resemble layers placed into a Z-shape.

Next, the cells are welded together complete with the placing the current collectors and finally welding the top cap. The electrolyte is filled using different holders through the aperture at the top cap. It is necessary to ensure that the electrolyte solution covers every pore in the internal structure and the separator membrane. After this step, the cells are conditioned outside the dry room.

The ***pouch cells*** were manufactured separately. The process lacked a standardized equipment and therefore, needed a lot of workforce and manual job initially. In the first step, the electrodes and the separators were cut into layers using a cutting press and stacked into layers of 38 anodes, 76 separators and 37 cathodes. The terminals were drawn out and tabs

were welded on them. The stacks thus formed were wrapped in two half-aluminium shells and heat sealed. The pouch cells were filled with the electrolyte solution in a glove box and the remaining side was welded. Then the cells were conditioned outside the dry room and the trapped gas bubbles in the structure were degassed as the last step.

(a) (b)

Figure 6. Packaging geometries of the cells manufactured (a) Prismatic (L), Cylindrical (R), (b) Pouch (Source: SPICY Deliverable 5.6)

The post manufacturing specifications of the cells are reported further in this subsection. The cell specifications of each geometry are mentioned in the following **Table 5**:

Table 5. Cell specification for cells of different geometries (Source: SPICY Deliverables 5.6)

	Cylindrical	Prismatic	Pouch
Lower Voltage limit (V)	2.5	2.5	2.5
Upper Voltage limit (V)	3.6	3.6	3.6
Maximum charge current (A)	50	4	50
Maximum discharge current (A)	100[1]	4***[2]	100[3]

[1] for a 30s pulse

[2] normal cycling, rate tests upto 12A

[3] for a 30s pulse

Temperature operation range (°C)	[-10, +55][4]	[0, +45]	[-10, +55]**[5]

The weight contribution of all the different components and the materials used to manufacture them are shown in **Table 6**. A clear difference is noticed in the cells with soft packaging, i.e. the pouch cells, due to softer casing.

Table 6. Weight contribution of different components of a cell characterised by cell packaging geometry (SOURCE: SPICY Deliverable 5.6)

Weight (g)	**Cylindrical (wound)**	**Prismatic (wound)**	**Pouch (soft casing)**	**Material**
Electrode collector	26.78	26.78	24.49	Al
	55.53	55.53	48.59	Cu
Component total	**82.31**	**82.31**	**73.08**	
Electrode coating	73.9	73.9	71.10	C
	5.93	5.93	5.63	Li
	43.94	43.94	41.69	Fe
	76.43	76.43	72.51	PO4
	9.15	9.15	6.12	Binder
Component total	**209.35**	**209.35**	**197.05**	
Electrolyte	11.74	11.74	11.10	LiPF6
	87.40	87.80	82.90	Carbonate
Component total	**99.14**	**99.54**	**94**	
Separator	11.30	11.30	10.45	Polypropylene
Mechanical parts (packaging, collectors, core, etc.)	46.54	85.19	7.70	Al
	5.06	31.41	3.80	Polypropylene
	20.88	22.04	6.01	Cu
	0.18	0.26	0.20	Ni
			1.50	Polyamid
			0.37	Other

[4] for charging [+5, +55]
[5] for charging [+5, +55]

Component total	**72.66**	**138.9**	**19.21**	
Total cell weight	**475**	**542**	**394**	

The weight results are documented as expected because of the hard cover being replaced by aluminum foil in the pouch cells, the packaging component and the overall cell weighs less. In the case of the prismatic cell, it requires more packaging than a cylindrical cell because of the higher surface area, as can be seen from the reception test data given in **Table 7**. The cells delivered were subjected to reception test and the data obtained are documented in the table:

Table 7. Cell geometry and reception test specifications (Source: Spicy_Reception_test_report_GEN0_September 2016_FZJ)

	Cylindrical	Prismatic	Pouch
Energy density (Wh/kg)[6]	108.61	94.25	121.77
Capacity (Ah)	16.099	15.963	14.889
Weight (g)[7]	474.32	541.98	391.25
Height (mm)	125	125	-
Curved Surface area (mm^2)	19625[8]	31250[9]	-
Nominal voltage (V)	3.2	3.2	3.2[10]

The data presented above were mentioned immediately after receiving the cells without any ageing. After that the cells were aged and cycled at different stages of State of Health (SOH). The following the section enumerates the different tests performed relevant to the current work.

4.3. Tests performed

[6] Energy density, $E = \frac{Q \times V_{nom}}{m}$, where Q = Capacity, V_{nom} = nominal voltage, m = mass

[7] the weight differs from value in **Table 5** because the reception test results mentioned refer only to the cells chosen to be tested within the scope of this work.

[8] Curved surface area of cylindrical cell = $2\pi rh$

[9] Curved surface area of prismatic cell, considered to be cuboidal = $2(l + b)h$

[10] The nominal voltage for pouch could not be found from the data but for uniformity it has been assumed to be almost equal to prismatic and cylindrical.

Overall all the cells are subjected to calendar life tests, cycle life tests and electrochemical impedance spectrometry (EIS). This thesis covers only the cycle life testing within its scope. It involves testing of the cells at different charging/discharging rates at different conditions of temperature over different states of health (SOH) or ageing time. In the cycle tests, the equivalent full cycles are observed over the ageing of the cells.

In both calendar life and cycle life tests, two kinds of checks are given – short check-up (SCU) and extended check-up (ECU). The extended check-ups (ECUs) involve the measurements of capacity evolution, open circuit voltages (OCV) and internal resistances by pulse tests. Another test involves the temperature developed at the first ECU for different charging and discharging rates. Within the scope of this thesis, the capacity evolution, the internal resistance developed at different capacities (pulse tests) and the temperature are the most interesting.

The tests were carried out using the Extended Cell Test System (XCTS), shown in **Figure 7** below, provided by BaSyTec GmbH. According to the BaSyTec XCTS product brochure, it is a lithium ion cell formation and test system with up to 25A or 50A. It has the further advantage of low working expenses because of the option of energy recovery heat generation. Using the 50A system, currents up to 300A can be produced because of parallel operation facility. The system control is done using the high speed and precision BaSyTest software. Due to such features, this system finds application in test of large Li-ion cells, high power tests, pulse tests and formation of lithium ion cells. (Include reference of BASyTec XCTS brochure here)

Figure 7. BaSyTec Extended Cell Test System (Source: BaSyTec GmbH, coutesy: http://www.alvatek.co.uk)

The life-cycle test standards are documented in Spicy Deliverable 6.1. The usual test conditions as mentioned in this deliverable can be enumerated as follows (include Spicy Deliverable 6.1 reference):

i. The state of charge calculated is the capacity calculated at usual discharge rate of 1C at 25°C.
ii. The state of health (SOH) refers only to the battery capacity decrease.
iii. The usual test conditions of C-rates for charging are 1, 2 and 3C, whereas for discharging are 1, 2, 3, …., 6C
iv. For this work, the SOC window for cycling is 0% to 100%
v. The end of life (EOL) is set to 80% of initial capacity, so most test results in this work contains values for a minimum SOC around 80%.

The following sub-sections cover the tests performed on the cells which are relevant within the course of the present work.

4.3.1. Capacity evolution of the cells

This test is done to gauge the performance of the cells over a certain ageing period. Of special interest is the capacity deterioration over time and the possible number of equivalent full cycles (EFC). The capacity deterioration is measured as SOH drop.

As mentioned earlier in the discussion of the test conditions (SPICY Deliverable 6.1), the state of health (SOH) refers only to the battery capacity decrease. The SOH is not a well-defined physical quantity. It can be defined and determined by using any measurable quantity that changes with ageing of the cell for example capacity, internal resistance, cell impedance, cycling temperature gradient changes etc., and is monitored with respect to the values for a new cell. Therefore, such details are not provided by the manufacturers and have to be independently determined by the testing infrastructure. There is no precise definition of SOH agreed upon uniformly by industries or scientists (M. Nisvo Ramadan et al. 2016). The SOH estimation within this work, as mentioned, has been done by measuring changes in the capacity of a fully charged cell. It can be depicted using the following equation:

$$(\text{M. Nisvo Ramadan et al. 2016})\ SOH = 1 - \frac{Q_{full,aged}}{Q_{full,new}}$$

Here, $Q_{full,aged}$ refers to the capacity of the aged (current state) battery at full charge (that is an SOC of 100%), while, $Q_{full,new}$ refers to the capacity of a new unaged battery at 100% SOC.

There are many different methods to calculate the capacity of the cell, for e.g. coulomb counting and open circuit voltage method (M. Nisvo Ramadan et al. 2016). But discussions of these methods are beyond the scope of this work.

For this work, the method for the capacity evolution and the subsequent SOH calculation is described below with the help of **Figure 8**. The figure shows a sample plot taken from a cylindrical cylinder testing. It helps to show how the SOH is being calculated. The cells were charged and discharged using the conventional constant current – constant voltage (CC+CV) and constant voltage (CV) protocols. (Li et al. 2011) The CC+CV protocol is the most popular charging protocol which involves a low rate constant current charging to a predefined cut-off voltage followed by float charging at the cut-off voltage until the current drops to very low preset value. The positive current and instantaneous capacities are for charging, while the negative values depict discharging.

i. An un-aged cell is discharged completely and the residual capacity is measured and noted.
ii. Next the cell is charged again first with constant current (CC) and then with constant current + constant voltage (CC+CV). When the cell is fully charged, the capacity is measured again and noted.
iii. This fully charged cell is discharged again and another discharge cycle, as described in step ii above, is carried out.
iv. The cell is again charged again and the cell capacity after the second discharge is noted, as saved as the $Cap_{reference}$ (reference initial capacity) of the unaged cell. This corresponds to the capacity at 100% SOH.
v. Steps i through iv are repeated for the aged cell and the cell capacity after the second discharging-charging step is noted and saved as $Cap_{i,aged}$ (the capacity of the aged cell at the ith step). The SOH of the aged cell is calculated using the following formula:

$$SOH_i = \frac{Cap_{i,aged}}{Cap_{reference}} \times 100$$

where, SOH_i is the state of health at the ith step

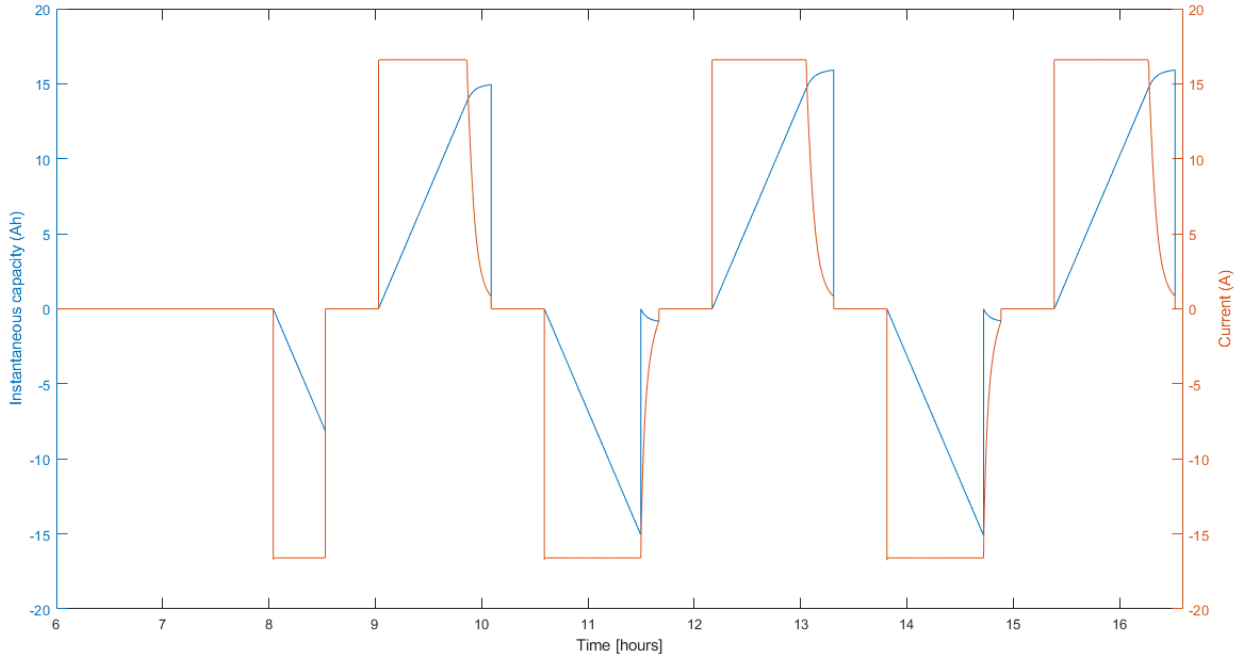

Figure 8. A sample plot to show the capacity evolution for the calculation of SOH

An aged cell has reduced full capacity and the number of full cycles it has gone through its life is not a linear curve with linear multiplicity. This quantity is defined by the term equivalent full cycles (EFC). The EFC can be calculated using the formula given below:

$$N_{eq} = \frac{W_{tot}}{2 \times U_{nom} \times Q_{init}}$$

….Equation 3, (Svens et al. 2015)

Here, N_{eq} = equivalent full cycles, W_{tot} = accumulated energy throughput for the cycled cell, U_{nom} = specified nominal battery voltage, Q_{init} = measured initial battery capacity

The capacity evolution or deterioration is studied with respect to changes in SOH and equivalent cull cycles (EFC). These conditions are checked for the cells of the three geometries for different conditions of temperature and cycling current rates. These results are discussed in the next chapter.

4.3.2. Temperature developed over cycling

To determine the temperature gradient over the three geometries at similar conditions, the temperatures were measured for the first extended check-up (ECU) cycle with different cycling current rates. In all the cases though, the charging was done with a rate 1C, but the discharging was tested with slow to fast cycling.

The temperature sensors used for the tests were the Negative Temperature Coefficient (NTC) sensors. This is the most commonly used type of temperature sensors, and in this case, the temperature shows an inverse relation with respect to the resistance. (Liu et al. 2018) NTC thermistors are high precision and can give a resolution and accuracy as low as 5mK.[11]

The different stages of the charging and discharging were identified by using the data for the cell voltage during the same stages. For demonstrating how the open circuit voltage changes at different stages of charging and discharging, the **Figure 9** is plotted to show the open circuit voltage at different stages of SOC while charging and discharging for different steps of extended check-ups (ECU) and short check-ups (SCU). This representation in the figure is a sample taken from test observation data available with SPICY. It must be noted that these are the open circuit voltages, while the cell voltages during continuous cycling differs from this data.

In the next chapter, these experimental observations are further analyzed with respect to check the temperature gradient and temperature peaks developed for each geometry.

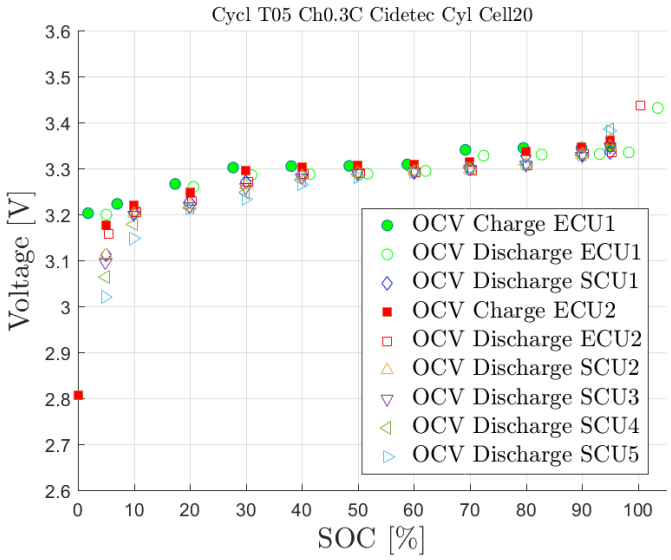

(a)

[11] The temperature sensor data has the potential to be improved by using embedded temperature sensors in the case of pouch cells or temperature sensors in the jelly roll structure of the prismatic and cylindrical cells

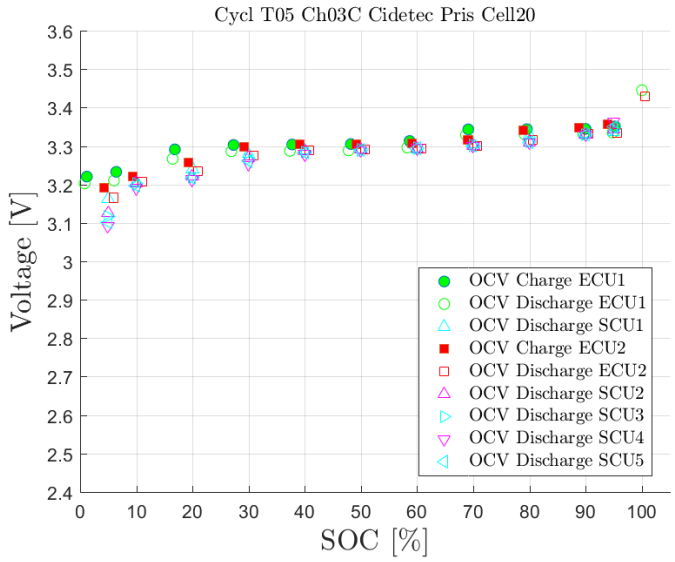

(b)

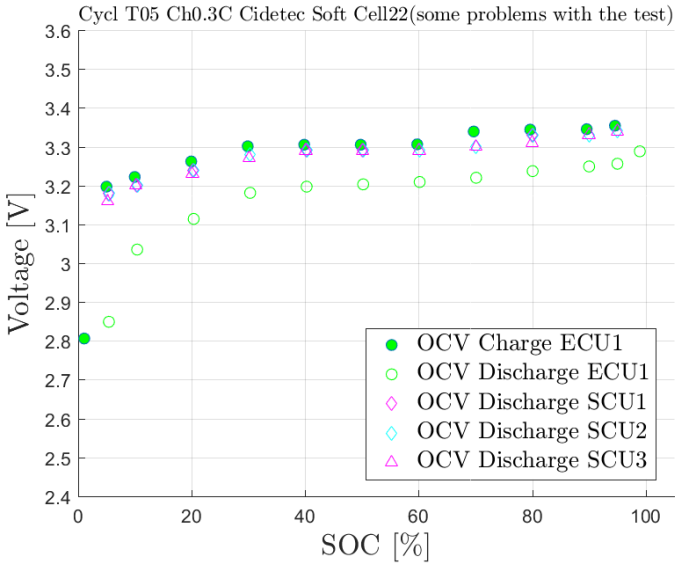

(c)

Figure 9. Sample data for OCV developed for charging and discharging (SOC) for (a) Cylindrical, (b) Prsimatic, (c) Pouch cells (Source: SPICY Test Observations)

4.3.3. Internal resistance calculation and pulse test

Internal resistance is one of the physical quantities which changes with ageing of the cell (expected increase) and it also gives information about the chemical changes within the cell. In this work, the internal resistance has been calculated for 30s charge and discharge pulses at the 0.5s, 10s and 30s time-instants. This section discussed the internal resistance measuring method followed by a discussion of the significance of the resistance values.

The internal resistance has simply been calculated by dividing the voltage and current at certain time instants. The pulses appear in two forms. While charging, first the SOC is determined for a fully discharged cell and a pulse of 1C is applied for 30s at that SOC. Next, the cell

stabilizes for a while without a pulse and then it is charged again at 1C this time to increase its SOC. In the case of discharging, the only difference is that a current is drawn from the cell. This is explained using **Figure 10** and **Figure 11**.

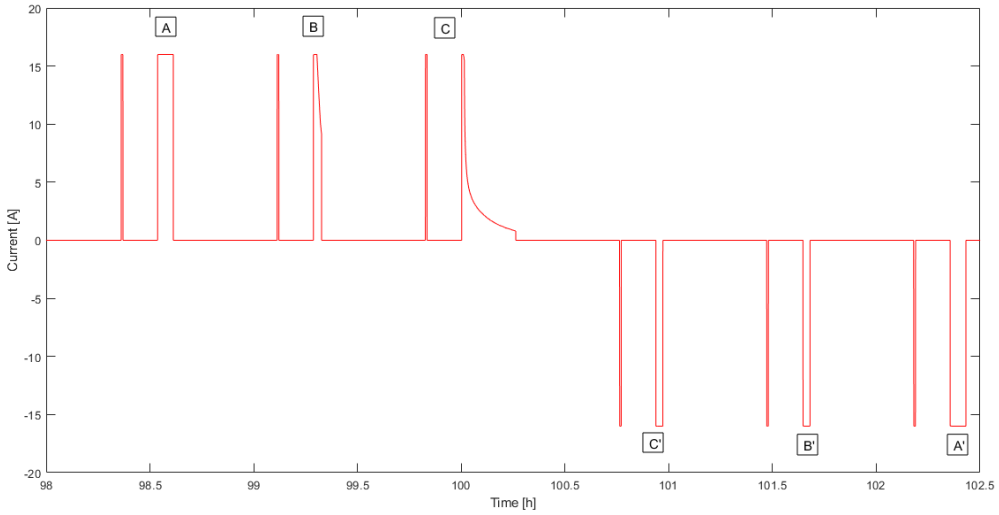

Figure 10. Charging and discharging current pulses for internal resistance tests for a prismatic cell.

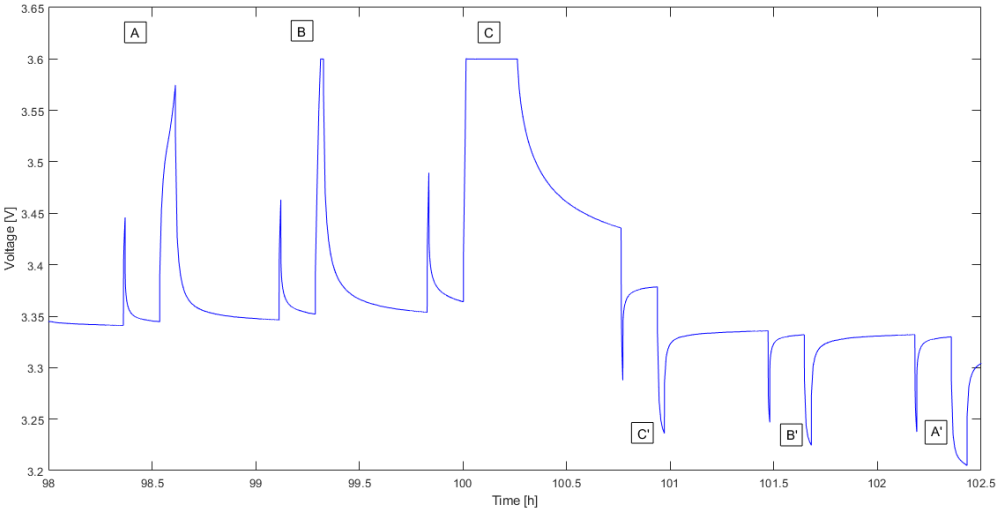

Figure 11. Voltage corresponding to the charge and discharge pulses

The data represented in **Figure 10** and **Figure 11** above is for a prismatic cell, but the same procedure is used for the other geometries as well. In the figures, the labels A, B, C, C', B', A' refer to one SOC step, each consisting of two pulses - the shorter pulse for 30s pulse test and the longer pulse for the SOC increase step. For the given figures, the **Table 8** represents the SOC changes and the currents involved for the longer current pulses with respect to each label:

Table 8. SOC change and pulse duration for SOC step in Figure 10

Label	SOC change	Pulse duration for SOC step[12]
A	80-90%	4.2s charge
B	90-95%	2.1s charge
C	95-100%	2.1s charge
C'	100-95%	2.1s discharge
B'	95-90%	2.1s discharge
A'	90-80%	4.2s discharge

Please note that the values given in **Table 8** only represents the corresponding values obtained from the plot represented in **Figure 10**. The pulse duration for a 10% SOC change is about ~4.2s, while for the 5% SOC change step, it is ~2.1s. Please note that the pulse duration of SOC change step may differ from one cell to another depending on the small differences between the capacities of the cells and depending on ageing influences.

A similar method of SOC change pulse and a shorter 30s pulse are used for the pulse test at the SOCs (charging and discharging, both): 5%, 10%, 20%, 30%, 40%, 50%, 60%, 70%, 80, 90% and 95%.

Further, for each 30s pulse, the internal resistance is calculated at the 0.5s, the 10s and 30s instant. This is done by calculating the instantaneous change of voltage in **Figure 11** and dividing it by the current at that time in **Figure 10** (which is approximately equal to 1C), as shown in the formula below:

$$IR = \frac{\frac{\partial V}{\partial t}}{I} dt$$

Where, ∂V refers to the infinitesimal change in voltage over ∂t in **Figure 11** and I refers to the current at the stage (which is usually constant at 1C or 16A)

The internal resistances of the cells at different time instant determine electrochemical activity of the cells. The polarization curve helps understand the significance of these resistances. The following figure represents a polarization curve of two (non-Lithium) electrochemical cells.

[12] Approximate time step values directly calculated from **Figure 10**

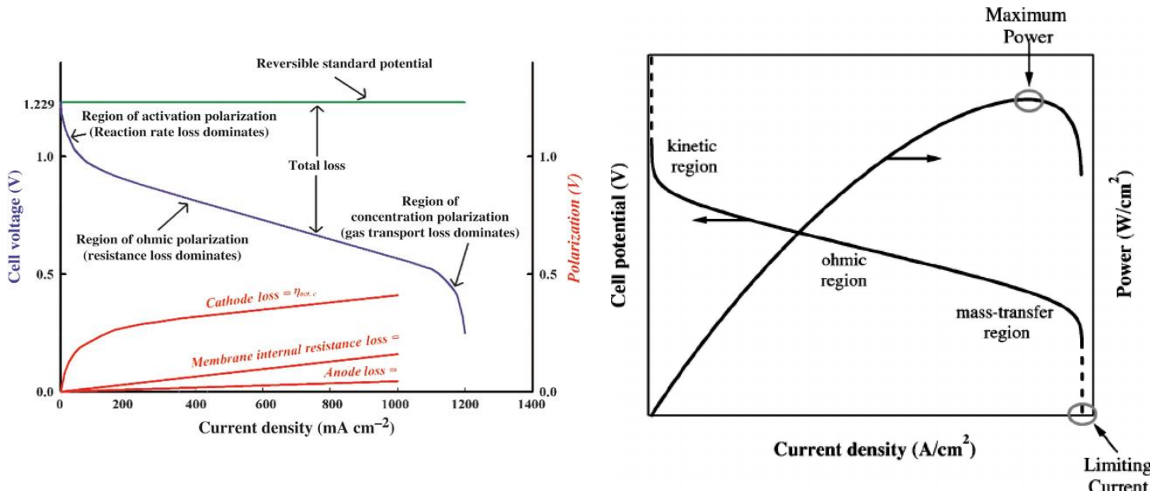

(a) (b)

Figure 12. (a) (Zhang et al. 2015) A typical polarization curve describes the relationship between cell voltage and current density used to evaluate cell performance of a PEMFC cell, (b) (Weber et al. 2004) Example polarization and power curves for a PEMFC cell

Figure 12 shows the discharge polarization curves (current density vs voltage) for polymer-electrolyte membrane fuel cells (PEMFCs) from the work done by (Zhang et al. 2015) and (Weber et al. 2004). The polarization curve here can be divided into three parts, namely, (a) the activation part representing the kinetic region, (b) the ohmic part representing the ionic exchange, and (c) the concentration part representing the mass-transfer region. (DuBeshter and Jorne 2017) In a fuel cell, the polarization curves give essential information about the governing performance for the different operating conditions of the cell, for example, at low current density, the performance of PEMFC is governed by positive electrode kinetic losses. But the difference between fuel cells and Li-ion cells is that while fuel cells operate in steady state, Li-ion cells have unsteady operation, i.e., the SOC of Li-ion changes while charging or discharging. (DuBeshter and Jorne 2017) Therefore, it is difficult to study battery voltage versus current density for the case of Li-ion batteries. But according to DuBeshter and Jorne, a method has been design to adapt polarization curve from fuel cells to Lithium-ion batteries in order to understand the governing factors of battery performance under various operating conditions at different SOCs (DuBeshter and Jorne 2017).

The adapted method can be used to give information about the charge transfer kinetics, ionic mass transport and solid-state diffusion. According to this method, for the pulse test, different time instants of the pulse represents different parts of the three governing factors. To create pulse polarization curve using this method, the end SOC must remain constant and that is the reason why the pulse test explained above is performed at a constant SOC.

Following this, DuBeshter and Jorne 2017 separated the overpotentials as mentioned in **Figure 12** for the lithium-ion batteries using the formula given below:

$$(\text{DuBeshter and Jorne 2017})\ \tau_s = \frac{L^2}{D}$$

where, τ_s refers to the time scale, L is the characteristic length, D is the diffusion coefficient. Using this information, it has been determined that for the 30s pulse test:

- The 0.5s instant represents the kinetics
- The 10s instant represents the electrolyte Li-ion concentration gradient
- The 30s instant represents the li solid state diffusion

Further, the internal resistance at these instants for each SOC represents the slope of the pulse polarization curve at that instant. This internal resistance value is plotted and studied for all the three different geometries of Li-ion batteries in the next chapter.

5. Results and discussions

MATLAB Data Processing and Visualization was used to extract, sort, edit and visualize the experimental data for ease of analysis. It was found that the data for cells under the same conditions of cycling rate and temperature show similar results and therefore the cell data were averaged. Further, in certain cases, data interpolation and extrapolation to maintain uniformity. The following sub-sections would discuss the experiment results from the previous chapter along with any assumptions made in each case.

An initial discussion of the cell chemistry and materials done in sub-section 2.2 (Starting from page 19) shows the measured values for parameters like cell weights, capacity and energy densities. It was already discussed a possible reason for the lower weight of the pouch cells due to its light-weight aluminum pouch cover and lack of any hard covering. A weight analysis of the different components of the cells are also done in **Table 6**. The difference in the weights of the prismatic (heavier) and cylindrical cells can be explained using the higher surface area of cover for the case of the prismatic cells leading to higher requirement of metallic cover material. The added weight is the case of the prismatic cells can also be attributed to an added metallic/steel support for stability. (Maiser 2014) A further reason could be that in a pouch cell, the cathode, separators and anode are stacked instead of wound, as can be seen in **Figure 2**. This approach increases packaging density to the maximum and saves weight, thus increasing energy density of the cell. The packaging density when grouping cylindrical cells is low due to their round shape, and the cell case is comparatively heavy. (Maiser 2014)

Due to the weight comparisons as discussed, it is not surprising that energy density (Wh/kg) of pouch cells is the highest followed by cylindrical cells followed by prismatic cells. (Considering that all the cells have a capacity close to 16Ah and a nominal voltage has been assumed to be the same at 3.2V).

While all the cells have been manufactured to be around 16Ah, **Table 7** shows a minor difference in the capacities of the cells. While cylindrical and prismatic cells are almost equal to 16Ah (cylindrical slightly higher), the capacity of pouch cell is a little less than 15Ah. A look at the **Table 6** can provide a possible reason for it. It shows that weight of electrode collector + electrode coating + electrolyte material is clearly less in the case of pouch cells as compared to prismatic and cylindrical geometries. The less electrode + electrolyte content in pouch cells might explain the reduced capacity.

The next sections discuss first the performance of a new unaged cell with respect to internal resistance profiles from pulse test and then the temperature evolution over cycling of each

geometry. The section after that discusses the effect of ageing on the cells, namely, the capacity deterioration and equivalent full cycles at different conditions of temperature and cycling, and the influence of ageing on internal resistances. For ease of study and data representation, all the data values for the same geometry and same test conditions are averaged out.

5.1. Performance of unaged cells

The data obtained from the tests are then pre-processed by averaging the values for the same geometry and same test conditions (C-rate and temperature). Also, for simplicity, only the data for 0.3C-rate condition are considered.

5.1.1. Internal resistance at 100% SOH for different cell geometries

The unaged cells are subjected to the 30s pulse test as explained in section 2.3.3. This internal resistance data was calculated over different State of Charge (SOC) of the cycling process, to represent the pulse polarization curve at every SOC considered. The resulting data comparison between the different cell geometries at the same conditions is represented in **Figure 13** and **Figure 14**.

It can be seen from the figures that the internal resistance values for cylindrical and prismatic geometries are almost identical in most cases, though the values for pouch cells are much lower. It is interesting to note that there is a sharp drop in internal resistance value at the start of the charging pulse (around 0-10% SOC). A similar phenomenon is observed for pouch cells in the reverse direction in the case of the discharge pulse. While in most cases, the internal resistance values of prismatic and cylindrical are higher than pouch, at the end of the discharge cycle, there is a sharp increase in the internal resistance curve for the pouch cell to reach values quite higher than prismatic and cylinder.

It is also notable from **Figure 13** (charging pulse at 0.3C and 5°C) that there is a characteristic decrease in the value of internal resistance when approaching an SOC of 70% in all geometries at the instants 10s and 30s (though it is negligible at 0.5s). Similarly, from **Figure 14** (discharging pulse at 0.3C and 5°C), during the discharge process, there is sudden peak of internal resistance around the 70% SOC mark for all geometries.

It can be easily concluded from the figures that in general the internal resistances of cylindrical and prismatic cells are higher as expected, at very low SOC values, this parameter value is higher for the pouch cells. Since development of internal resistances is directly related to capacity losses, cylindrical and prismatic cells have higher capacity losses in general. But if

pouch cells are used at a lower SOC for longer period of times, this might lead to steeper capacity losses for it.

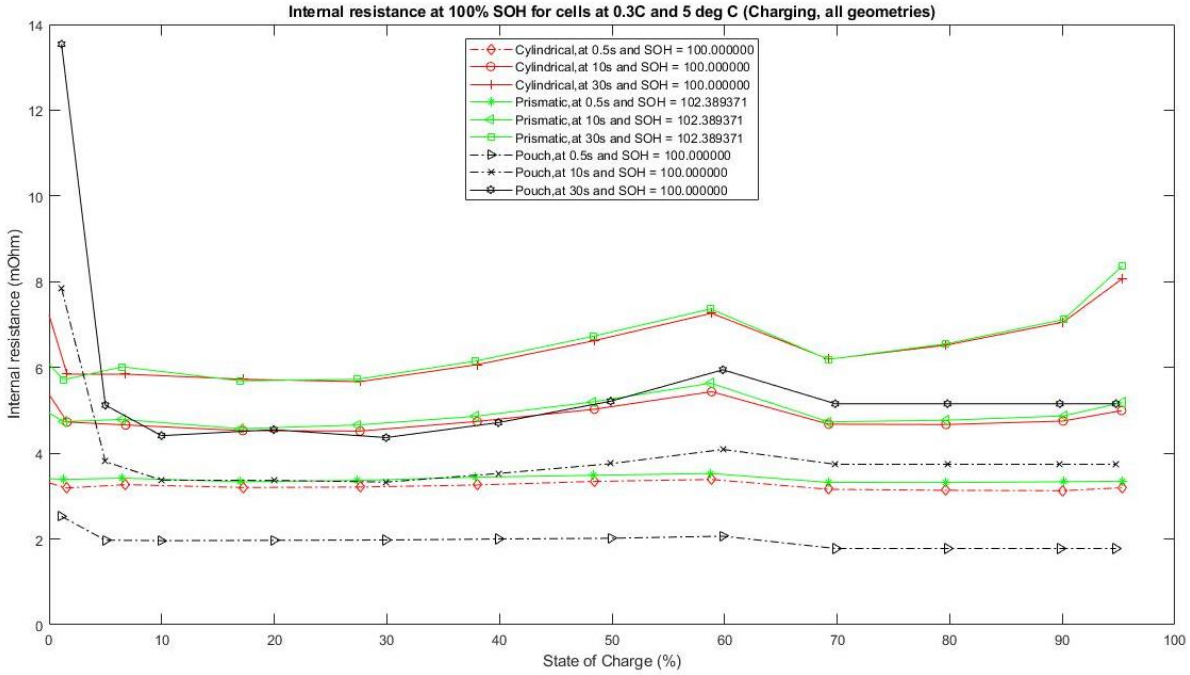

Figure 13. Internal resistance comparison at 100% (0.3C, 5°C and charging pulse)

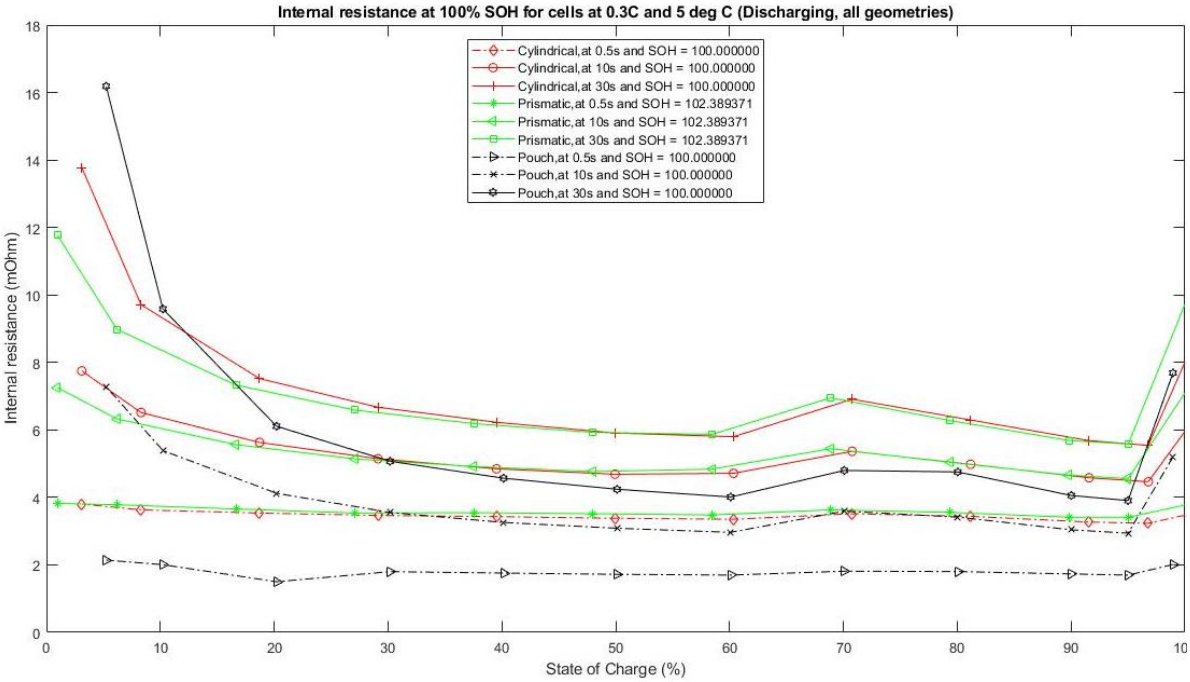

Figure 14. Internal resistance comparison at 100% (0.3C, 5°C and discharging pulse)

Table 9 below enumerates the values of internal resistance at the SOC values of 5%, 50% and 95%. It can be seen that neglecting the sudden surges in internal resistance in pouch

cells around the early SOC regions, the internal resistance follows the general trend of: prismatic >= cylindrical > pouch.

Table 9. Internal resistance of selected SOC stages for a charging pulse for all geometries.

Geometry	**5% (in mOhm)**			**50% (in mOhm)**			**95% (in mOhm)**		
Pulse instant	*0.5s*	*10s*	*30s*	*0.5s*	*10s*	*30s*	*0.5s*	*10s*	*30s*
Charging pulse for cells at 5°C/0.3C									
Cylindrical	3.241	4.682	5.845	3.343	5.026	6.626	3.196	4.995	8.059
Prismatic	3.411	4.773	5.929	3.486	5.197	6.727	3.349	5.183	8.367
Pouch	1.972	3.806	5.122	2.017	3.756	5.214	1.779	3.743	5.155
Discharging pulse for cells at 5°C/0.3C									
Cylindrical	3.741	7.299	12.294	3.381	4.686	5.909	3.225	4.455	5.530
Prismatic	3.792	6.538	9.616	3.516	4.764	5.927	3.411	4.558	5.582
Pouch	2.142	7.278	16.19	1.72	3.085	4.242	1.697	2.940	3.906

5.1.1.1. Temperature developed over cycling

One of the major safety issues in commercial Li-ion batteries especially in EV and HEV is associated with the temperature developed over the cycling period. Therefore, it becomes an important parameter for cell performance evaluation. Data for temperature developed is processed from the first ECU of unaged cells. For uniformity, the temperature profiles were plotted for cells stored at 0.3C and 5°C. During the cycling, the charging was done at 1C, but the discharge was done at 0.2C, 0.5C, 1C and 2C. **Figure 15** shows the temperature evolved over the cycles for the three geometries, along with the voltage of the cells to represent the cyclies.

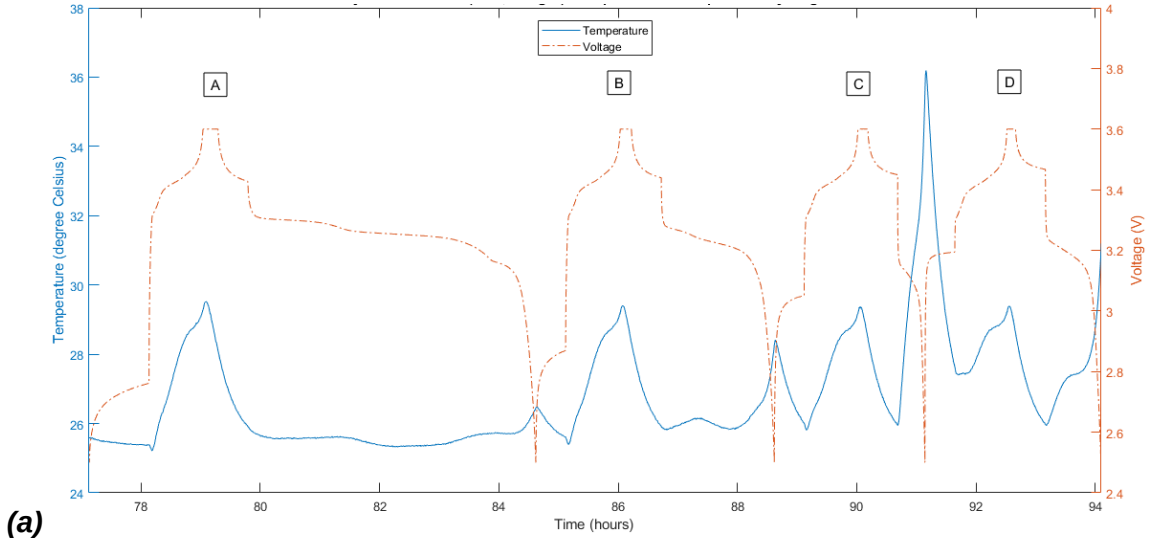

(a)

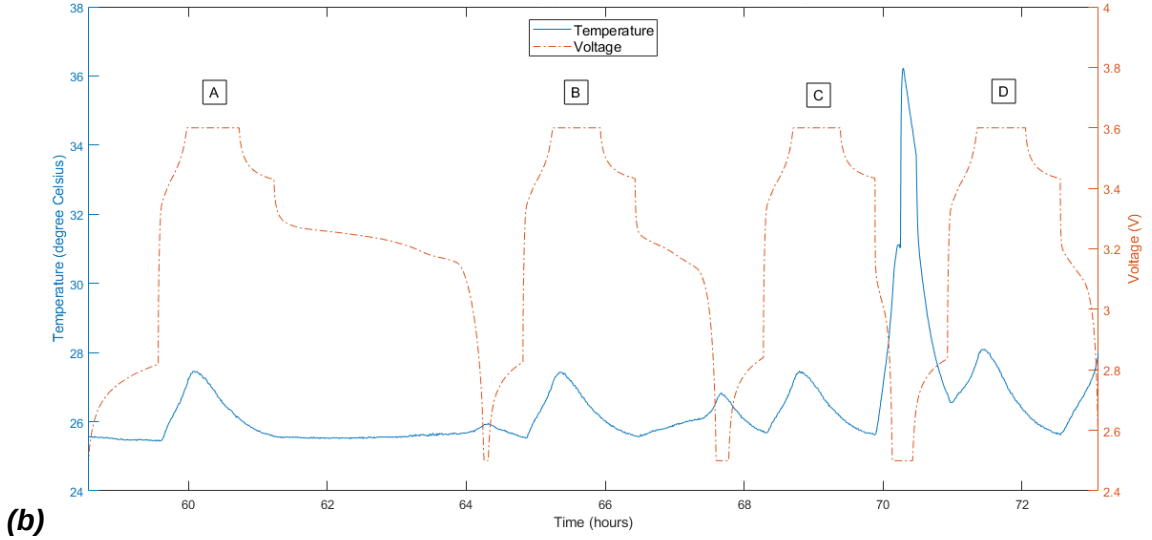

(b)

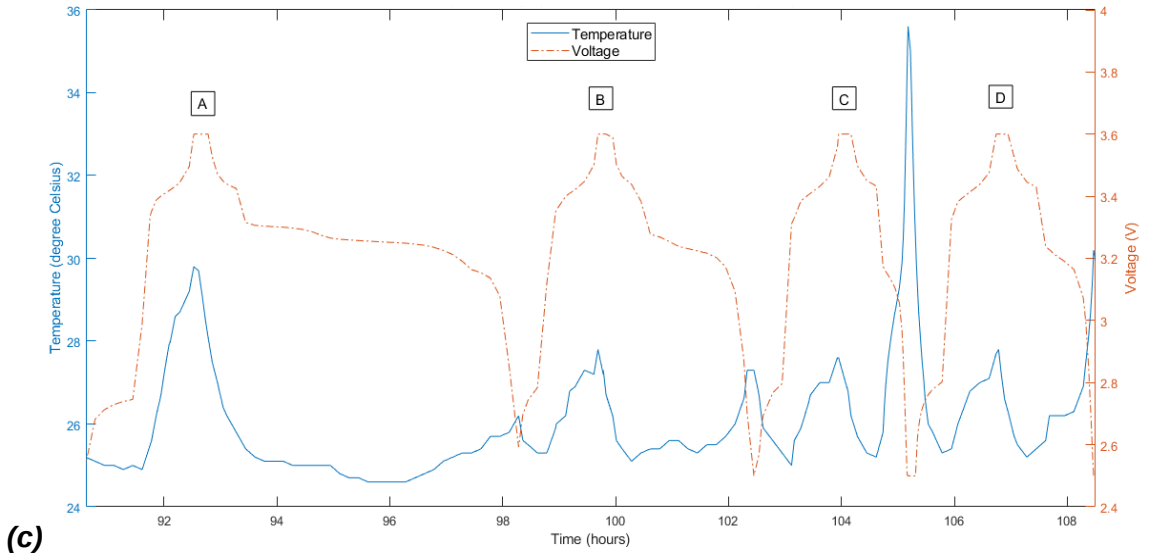

(c)

Figure 15. Temperature developed over cycling for (a) Cylindrical, (b) Prismatic, (c) Pouch cells

The labels in the figure refer to one cycle each and are characterised by the C-rates as shown in **Table 10**.

Table 10. Table showing the cycle characteristic denoted by labels in Figure 15

Label	**A**	**B**	**C**	**D**
Charging	1C	1C	1C	1C
Discharging	0.2C	0.5C	2C	1C

The temperature profile shows a common trend among all the geometries. There are two local peaks for each cycle, one at the end of the charging cycle and one at the end of the discharging cycle. The temperature at the end of the charging cycle (at the rate of 1C) remains almost same at the end of all the charging cycles, except for the first charging cycle of pouch cell where it is slightly higher than the subsequent cycles. **Table 11** shows the temperature gradient developed between the beginning of the charging cycle and the peak temperatures.

Table 11. Temperature gradient developed at different charge/discharge cycles for all geometries

Cell Type	**First 1C Charge (°C or K)**	**1C discharge (°C or K)**	**2C discharge (°C or K)**
Cylindrical	4.14	1.83	10.19
Prismatic	2	1.34	10.51
Pouch	4.8	2.5	10.30

The first column in the table shows the temperature gradient during the charging cycle at 1C (the local peak) with respect to the temperature at the beginning of the cycle, while the next two columns show the gradient at the end of 1C and 2C discharge with respect to the temperature at the start of the cycle.

A significant observation is the global peak in temperature developed at the end of the 1C charge - 2C discharge cyce for all geometries. The **Figure 16** below shows a a zoomed in section for this cycle on the same scaled axis. For each cell, the intitial temperature at the start of the whole cycle, the temperature peak at the end of the first charging cycle and

temperature peak at the end of discharge cycle are also mentioned. Please note that the difference in time scale is not a significant factor as all data is for the first ECU of all geometries.

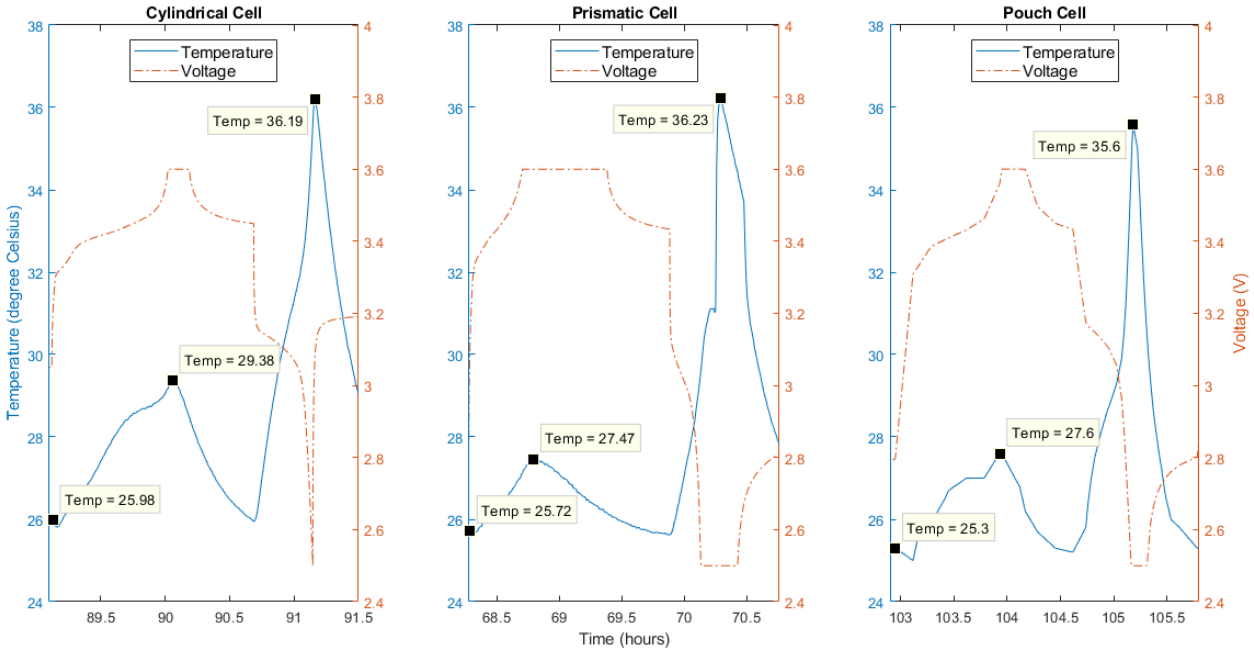

Figure 16. Temperature profile for 1C charge and 2C discharge for all three geometries.

The local peak temperature at the end of the charging for the case of the cylindrical cell is higher than the other two geometries. But, the maximum temperature developed in each case remains the most important parameter for this study. For the 1C charge-2C discharge case, while the temperature gradients are almost similar, the absolute temperature at the end of the 2C discharge is slightly lower for the pouch cell.

This is a reasonable conclusion since the problems with thermal management and a lack of proper passage for waste heat in prismatic cells are well known. This mostly because of the higher mechanical stresses. (Eric Maiser 2014) This leads to the temperatures building inside especially when subjected to rapid discharging currents. A cylindrical cell has the least surface area for heat dissipation (Zhao et al. 2016), which explains the higher temperatures developed in it. As discussed earlier, pouch cells usually use thin slices of electrodes and separators which are stacked in layers. Thin electrodes can enhance the fluency of ion diffusion and improve the electrochemical reactions which helps high rate discharges and long term performances due to the mild temperature variation (Zhao et al. 2016), which might also indicate the lower temperature developed in pouch cells and no rapid increase in temperature at 2C.

Summarizing the temperature profile results, it is observed that the peak temperatures are generated at the end of charging or at the end of discharging, while higher temperatures are

reached for higher C-rates. This is because over both charge and discharge, the Li ion migrate inside the cells to establish a concentration gradient, which generates heat as a function of applied current (Novais et al. 2016). These temperatures are higher at the end of the discharge, which increases with increase in discharge C-rate from 0.2C to 2C. It is expected that the temperature rise will be even higher at higher C-rates.

Better results can be expected by testing at discharge rates higher than 2C. Further a more comprehensive study can be done with monitoring the internal temperatures developed in the cells by using methods such as using embedded temperature sensors in the case of pouch cells or temperature sensors in the jelly roll structure of the prismatic and cylindrical cells.

[INCLUDE A CONCLUSION OF PERFORMANCE ANALYSIS OF THE CELL]

5.2. Ageing effects on cells of different geometries

The previous section discusses the performance of unaged cell. This section discusses the behavior of the cells during aging at the given temperature and C-rates. First, the capacity deterioration is discussed with respect to the equivalent full cycles (EFC). The next subsection discusses the effect of aging on the 30s pulse test results for the selected conditions of temperature and C-rates.

5.2.1.1. Ageing characteristics over equivalent full cycle (EFC)

The concept of equivalent full cycles (EFC) has already been discussed in section 2.3.1. Because of ageing, the way one whole full cycle is defined differs from one time-step to other. The capacity itself undergoes changes because of the cyclic and storage deterioration. Different cell chemistries therefore show different drop in capacities and different number of equivalent cycles possible over that the ageing period. **Error! Reference source not found.** shows the equivalent number of cycles for each geometry of cell for different cell conditions over the ageing period as shown by the State of Health (SOH). As discussed already, the SOH has been determined by drop of capacity of the cells, therefore SOH is used as the parameter to describe the ageing process.

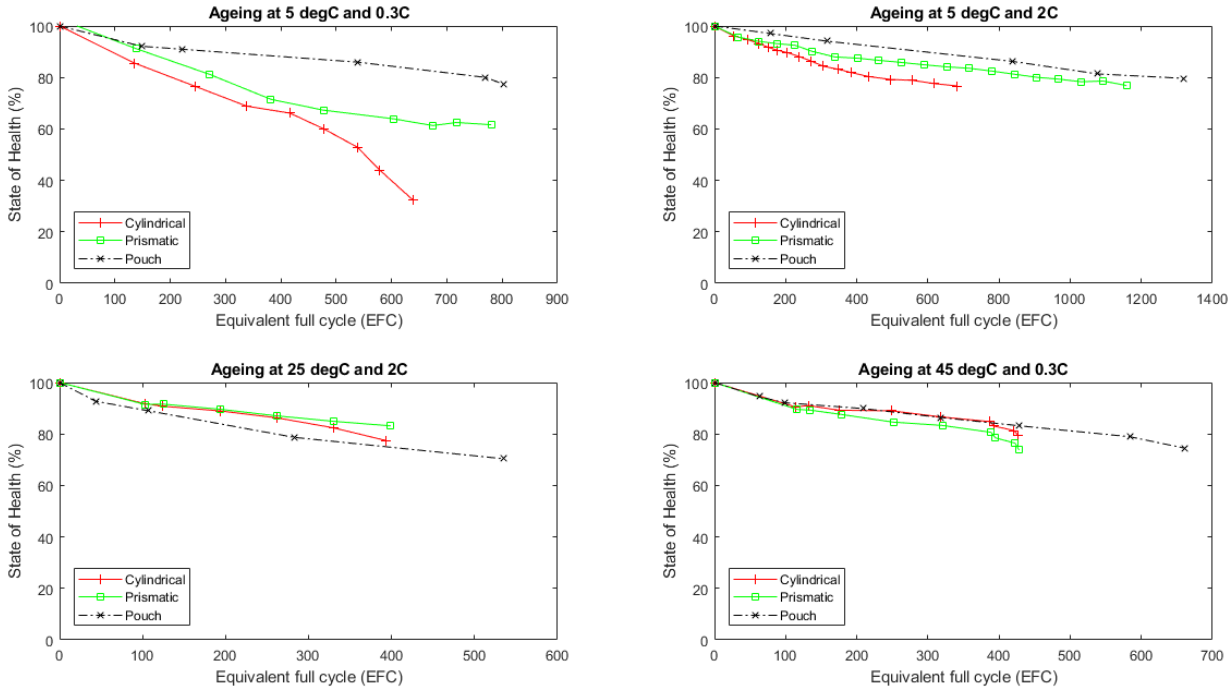

Figure 17. Capacity deterioration and the number of equivalent cycles obtained over the ageing period for different cycling conditions.

The curves show a downward parabolic to negative linear slopes in most cases. As expected, the equivalent full cycles do not show a simple arithmetic progression which may be wrongly assumed by considering the capacity to not change over the whole period. For the comparison of geometries, it is relevant to note the remaining capacities of the cell geometries after a certain number of effective full cycles.

Table 12 shows the remaining capacity of each cell geometry after 400 EFCs under different cycling conditions:

Table 12. Table showing the remaining capacities of cells, in terms of SOH, after 400 cycles (EFC)

Cycling conditions	Remaining capacity in terms of SOH after 400 EFCs (%)		
	Cylindrical	Prismatic	Pouch
5°C, 0.3C	66.69	70.70	88.13
5°C, 2C	81.40	87.49	92.84
25°C, 2C	76.94	83.12	74.82
45°C, 0.3C	82.63	78.10	84.02

For cylindrical cells, it is observed that an increase in C-rate of cycling reduces the capacity drop of the cell while the number of equivalent full cycles almost remain. Further, an increase in temperature has marginal change on the number of equivalent full cycles (marginal decrease at 25°C from 5°C and marginal increase at 45°C from 25°C), whereas the capacity loss remains almost the same.

For prismatic cells, an increase in C-rate of cycling increases significantly the equivalent full cycles and reduces the capacity deterioration as well. But an increase in temperature from 5°C to 25°C significantly brings down the number of equivalent full cycles, while the capacity deterioration almost remains the same. There is a further decrease in equivalent full cycles when the temperature is increased to 45°C, while the capacity deterioration is almost unchanged.

The pouch geometry shows a low capacity deterioration in all conditions of temperature and C-rate, and it also does not undergo a big change. It also has a higher number of equivalent full cycles in all cases as compared to cylindrical and prismatic geometries. An increase in C-rate has a significant increase in the equivalent full cycles, though it drops down when the temperature is increased from 5°C to 25°C.

In conclusion, it can be inferred from these results that for cylindrical geometry goes through improvement in number of cycles and less deterioration in capacity by an increase in C-rate of cycling. For the prismatic packaging, C-rate has significant improvement in cycles numbers and its life as well, while an increase in temperature has a negative impact on cycles. Pouch cells have the best ageing performance under the given conditions with respect to cylindrical and pouch cells. It has a good life in all conditions but goes through a loss of cycles at elevated temperatures.

5.2.1.2. Change in internal resistance by ageing (during a charging/discharging pulse)

Ageing leads to an increase in internal resistance and higher the resistance increase higher is the capacity loss of the cell/ Therefore, it is more interesting to note the incremental change in internal resistance over ageing period on the different cell geometries. This section analyzed the incremental change in internal resistance during charging and discharging. The plots with the absolute values of internal resistances can be found in

References

There are no sources in the current document.

Figure 18, **Figure 19** and **Figure 20** show the incremental change in internal resistance of a cell during a 30s charging pulse at different instants of 0.5s, 10s and 30s, compared over different geometries stored at different temperatures. The incremental change is calculated by taking the ratio of the internal resistance of the cell at an aged stage with respect to the internal resistance at 100% State of Health (SOH) or unaged stage.

A very first observation shows that a pouch cell at elevated temperatures (45°C) shows a positive change, that is a reduction in the internal resistance value (ratio less than 1) at all time instants of measurement. Whereas a prismatic cell at the same temperature shows the highest increase in internal resistance value at almost all measurement, though the difference is negligible compared to the other geometries. **Table 13** shows that the increment is highest for the prismatic cell stored at 45°C with a value of 1.394, while the pouch cell at 45°C shows a maximum decrease of almost by half.

However, on comparing the absolute values, it can also be seen that the internal resistance values for pouch cells under most conditions are the least.

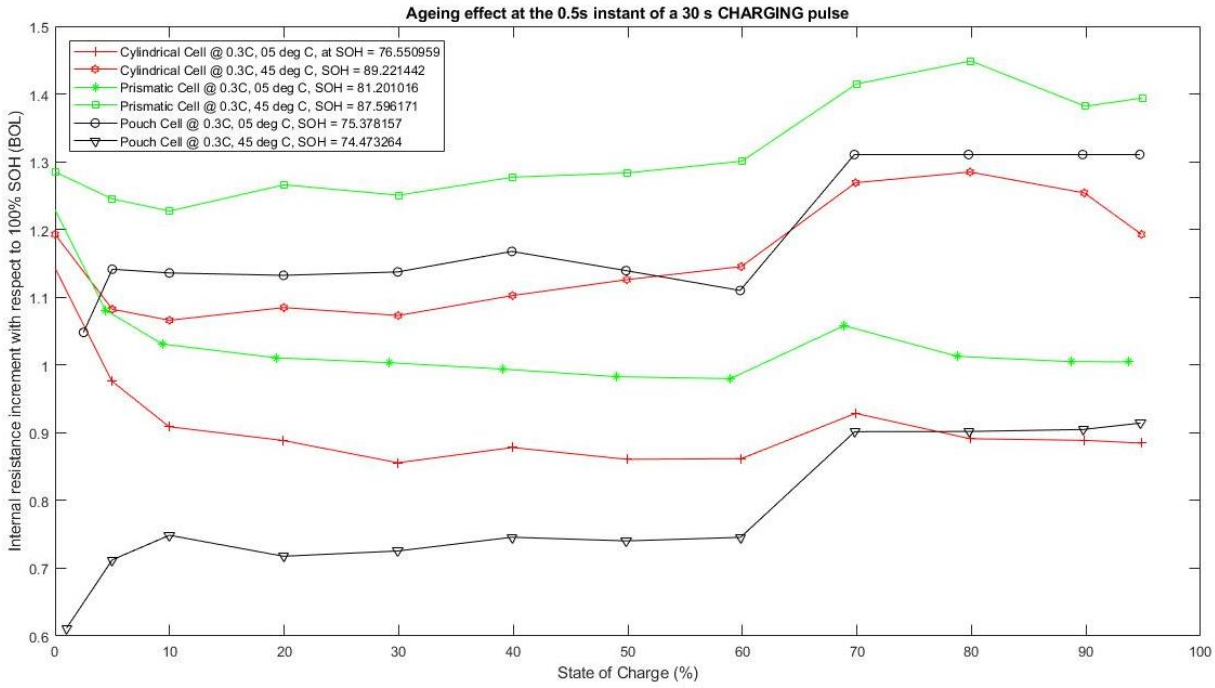

Figure 18. Incremental internal resistance (compared to 100% SOH) at the 0.5s instant of a 30s charging pulse.

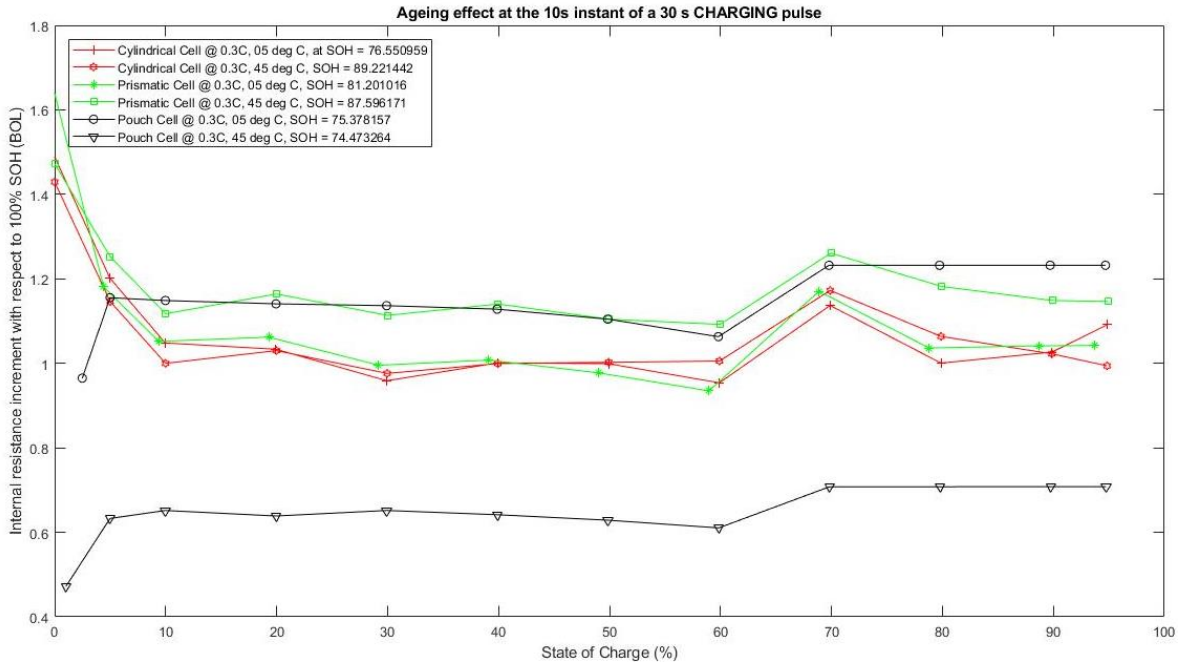

Figure 19. Incremental internal resistance (compared to 100% SOH) at the 10s instant of a 30s charging pulse.

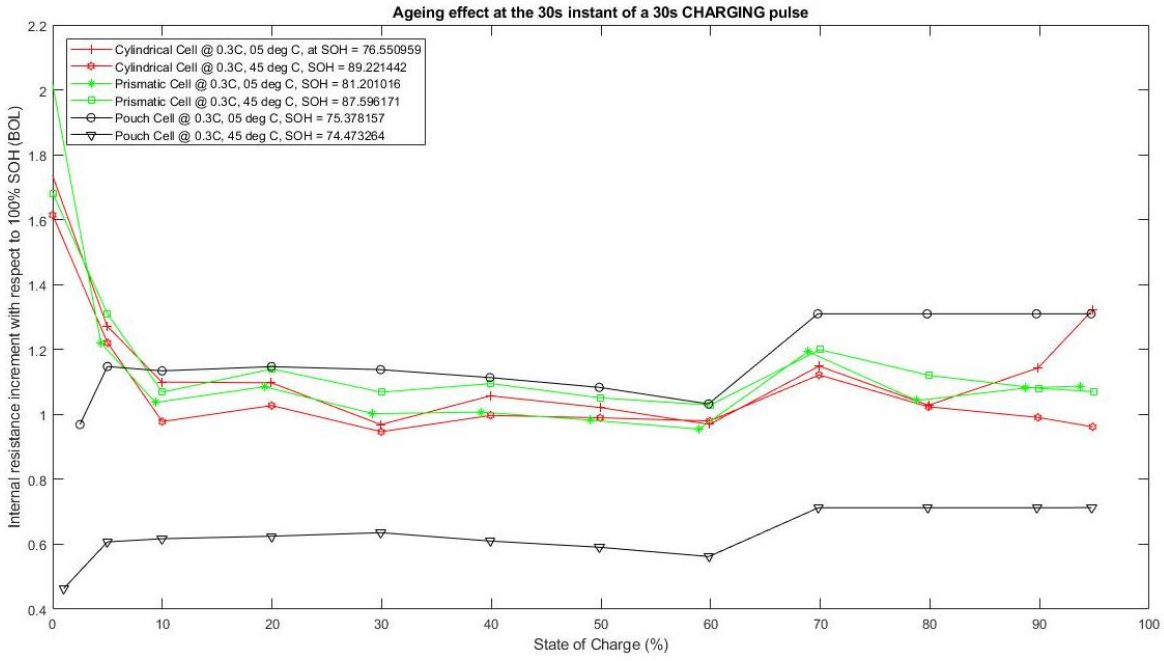

Figure 20. Incremental internal resistance (compared to 100% SOH) at the 30s instant of a 30s charging pulse.

Figure 22, **Figure 23** and **Figure 23** show the incremental change in internal resistance of a cell during a 30s discharging pulse at different instants of 0.5s, 10s and 30s, compared over different geometries stored at different temperatures.

For the discharge pulses, the internal resistances increase by less magnitude than in the case of charging pulse (max increase is 1.222) but the pouch cell at elevated temperatures shows a peculiar trend under a discharge pulse. At 45°C, the internal resistance value in the case of pouch cells shows a constant decrease as compared to the case at 100% SOH with a value up to almost 40% of the unaged cells. This can perhaps be explained by the results from the last section where the ageing of the pouch cells did not suffer by an increase in temperature or increase in C-rate. Therefore it brings a further stability to the functioning of the pouch type cells.

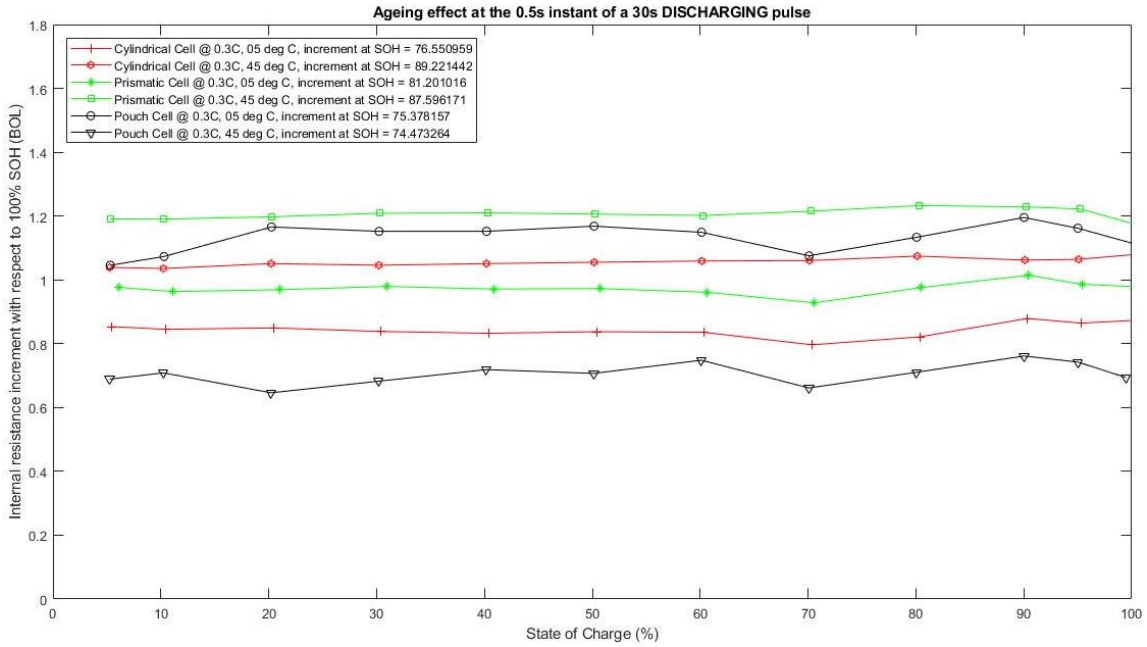

Figure 21. Incremental internal resistance (compared to 100% SOH) at the 0.5s instant of a 30s discharging pulse.

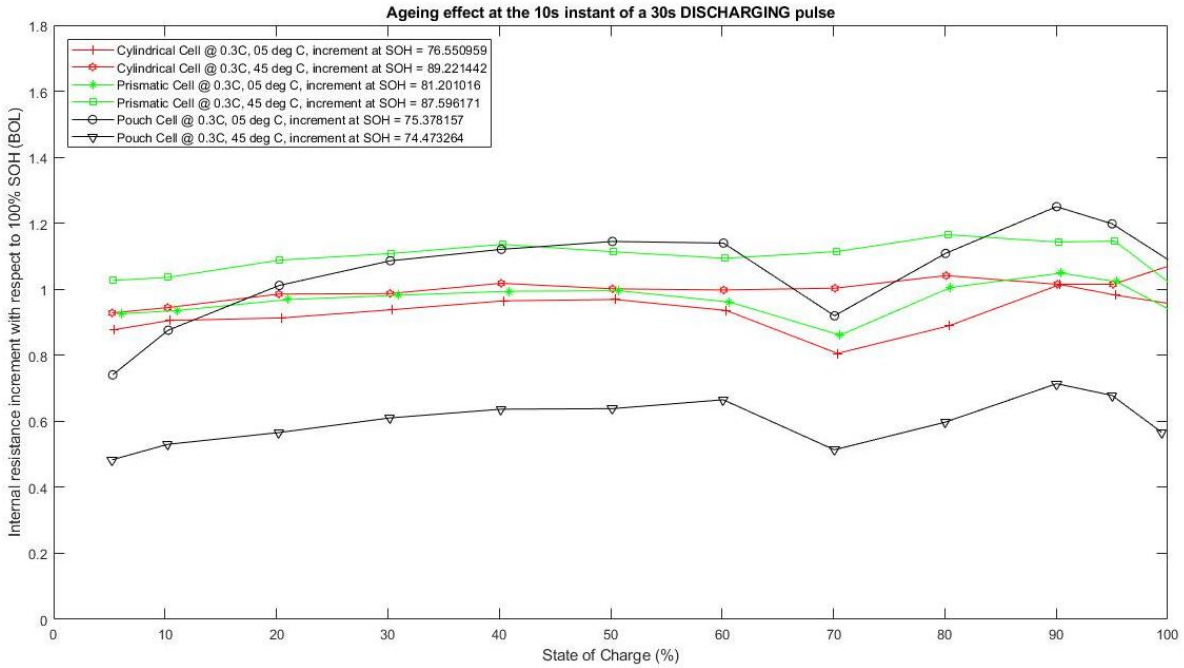

Figure 22. Incremental internal resistance (compared to 100% SOH) at the 10s instant of a 30s discharging pulse.

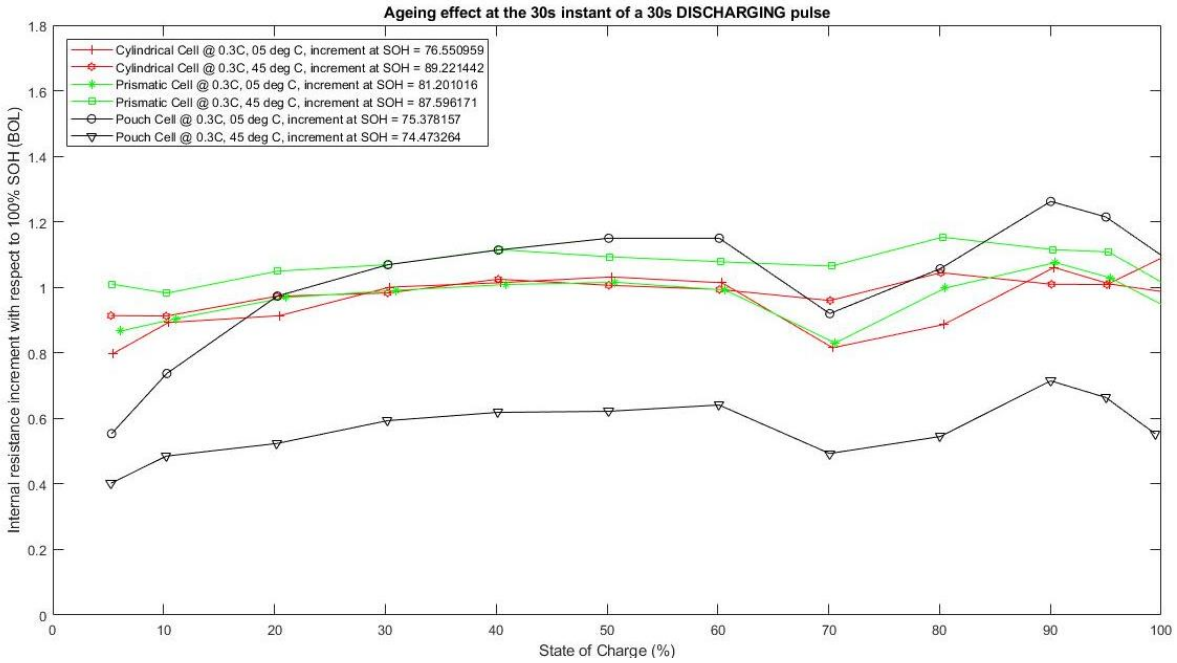

Figure 23. Incremental internal resistance (compared to 100% SOH) at the 30s instant of a 30s discharging pulse.

From the sections in page number 40 and page number 42, it can be inferred that the ageing of the cells can predicted based on internal resistance increment values and the effect of temperature and cycling on the equivalent cycle number and capacity drop. That is, a decrease in internal resistance in a 30s charge/discharge test may indicate a gradual deterioration or decay of the cell life as can be seen in the case of pouch cells

*NOTE: In **Table 13** and **Table 14**, the shaded rows refer to the increment ratio of the internal resistance, while the unshaded rows are the absolute values of internal resistance at the aged SOH mentioned with the geometry column. Cyl = Cylindrical, Pri = Prismatic, Po = Pouch*

Table 13. Changing in internal resistance due to ageing (for charging pulses)

	5%			**50%**			**95%**		
Pulse	*0.5s*	*10s*	*30s*	*0.5s*	*10s*	*30s*	*0.5s*	*10s*	*30s*
Charging pulse for cells at 5°C/0.3C									
Cyl	3.110	5.685	7.433	2.874	5.020	6.767	2.824	5.449	10.65
76.6%	*0.976*	***1.146***	***1.273***	*0.861*	***1.002***	***1.021***	*0.885*	*0.994*	***1.325***
Pri	3.630	5.580	6.980	3.426	5.08	6.610	3.370	5.450	9.110
81.2%	***1.081***	***1.252***	***1.196***	*0.983*	***1.104***	*0.979*	***1.005***	***1.146***	***1.087***
Po	2.244	4.393	5.867	2.296	4.149	5.649	2.325	4.608	6.750
75.4%	***1.141***	*0.633*	***1.147***	***1.139***	*0.629*	***1.083***	***1.311***	*0.708*	***1.310***
Charging pulse for cells at 45°C/0.3C									
Cy	2.877	4.666	6.125	2.820	4.325	5.804	2.657	4.193	6.544
89.2%	***1.082***	***1.202***	***1.221***	***1.126***	*0.999*	*0.990*	***1.193***	***1.091***	*0.962*
Pri	3.742	5.442	6.847	3.670	5.036	6.352	3.574	5.078	7.331
87.6%	***1.245***	***1.172***	***1.310***	***1.284***	*0.977*	***1.051***	***1.394***	***1.042***	***1.071***
Po	1.497	2.497	3.333	1.627	2.476	3.190	1.708	2.768	3.809
74.5%	*0.712*	***1.155***	*0.607*	*0.740*	***1.105***	*0.591*	*0.914*	***1.232***	*0.713*

Table 14. Changing in internal resistance due to ageing (for discharging pulses)

	5%			**50%**			**95%**		
Pulse	*0.5s*	*10s*	*30s*	*0.5s*	*10s*	*30s*	*0.5s*	*10s*	*30s*
Discharging pulse for cells at 5°C/0.3C									
Cyl	3.247	6.767	10.741	2.830	4.541	6.096	2.792	4.385	5.598
76.55 %	*0.853*	*0.877*	*0.798*	*0.837*	*0.965*	***1.031***	*0.864*	*0.982*	***1.010***
Pri	3.731	6.722	10.211	3.420	4.744	6.019	3.364	4.664	5.746
81.20 %	*0.976*	*0.926*	*0.866*	*0.972*	*0.994*	***1.015***	*0.986*	***1.023***	***1.029***
Po	2.150	4.720	7.070	2.010	3.532	4.878	1.972	3.524	4.745
	1.045	*0.740*	*0.553*	***1.168***	***1.120***	***1.149***	***1.161***	***1.198***	***1.214***

75.38 %									
Discharging pulse for cells at 45°C/0.3C									
Cy	3.029	5.641	8.909	2.748	3.991	5.221	2.701	3.858	4.901
89.22 %	***1.039***	*0.928*	*0.913*	***1.055***	***1.018***	***1.006***	***1.064***	***1.015***	***1.008***
Pri	3.890	6.387	9.567	3.630	4.802	5.927	3.564	4.649	5.591
87.60 %	***1.190***	***1.026***	***1.009***	***1.206***	***1.136***	***1.093***	***1.222***	***1.146***	***1.108***
Po	1.392	2.648	4.112	1.307	2.030	2.700	1.325	2.040	2.643
74.47 %	*0.689*	*0.483*	*0.402*	*0.707*	*0.636*	*0.621*	*0.742*	*0.678*	*0.663*

References

There are no sources in the current document.

APPENDIX

LIST OF FIGURES

LIST OF TABLES